Long non-coding RNA TINCR suppresses metastatic melanoma dissemination by preventing ATF4 translation

Marine Melixetian[1] (iD), Daniela Bossi[1,†], Marija Mihailovich[1], Simona Punzi[1,‡], Iros Barozzi[2], Federica Marocchi[1], Alessandro Cuomo[1], Tiziana Bonaldi[1] (iD), Giuseppe Testa[1,3] (iD), Jean-Christophe Marine[4,5], Eleonora Leucci[6], Saverio Minucci[1,7], Pier Giuseppe Pelicci[1,3,*] (iD) & Luisa Lanfrancone[1,**] (iD)

Abstract

Transition from proliferative-to-invasive phenotypes promotes metastasis and therapy resistance in melanoma. Reversion of the invasive phenotype, however, is challenged by the poor understanding of mechanisms underlying its maintenance. Here, we report that the lncRNA TINCR is down-regulated in metastatic melanoma and its silencing increases the expression levels of invasive markers, *in vitro* migration, *in vivo* tumor growth, and resistance to BRAF and MEK inhibitors. The critical mediator is ATF4, a central player of the integrated stress response (ISR), which is activated in TINCR-depleted cells in the absence of starvation and eIF2α phosphorylation. TINCR depletion increases global protein synthesis and induces translational reprogramming, leading to increased translation of mRNAs encoding ATF4 and other ISR proteins. Strikingly, re-expression of TINCR in metastatic melanoma suppresses the invasive phenotype, reduces numbers of tumor-initiating cells and metastasis formation, and increases drug sensitivity. Mechanistically, TINCR interacts with mRNAs associated with the invasive phenotype, including ATF4, preventing their binding to ribosomes. Thus, TINCR is a suppressor of the melanoma invasive phenotype, which functions in nutrient-rich conditions by repressing translation of selected ISR RNAs.

Introduction

Cutaneous melanoma is the most aggressive form of skin cancer, mainly due to early metastasization and rapid development of resistance to available treatments (Kunz & Holzel, 2017; Schadendorf *et al*, 2018). Metastatic dissemination is connected to the high propensity of melanoma cells to migrate and invade neighboring tissue, a property that is acquired since the earliest steps of melanomagenesis (Damsky *et al*, 2014). Though treatment of metastatic melanoma has been revolutionized in the recent years, thanks to the use of targeted therapies (such as BRAF[V600E] or MAP-kinase inhibitors) and immune checkpoint (PD-1 or CTLA-4) inhibitors (Landsberg *et al*, 2012; Woods *et al*, 2014; Hugo *et al*, 2016; Tirosh *et al*, 2016b; Jaberg-Bentele *et al*, 2017; Kunz & Holzel, 2017), the response rate to either treatments is less than 50%, with a relapse rate near 100% with targeted treatments and ~ 30% with immunotherapy (Damsky *et al*, 2014; Kunz & Holzel, 2017; Schadendorf *et al*, 2018; Garcia-Jimenez & Goding, 2019).

Emerging evidence indicates that metastasization and drug resistance result from the capacity of melanoma cells to dynamically change their phenotype in response to environmental perturbations, so called phenotype plasticity (Rambow *et al*, 2019). Melanoma cells can in fact reprogram transcription and metabolism in response to nutrient deprivation or extracellular signals from the tumor microenvironment (TME), resulting into the generation of distinct cell phenotypes and high degree of intratumor heterogeneity (Falletta *et al*, 2017; Ferguson *et al*, 2017; Garcia-Jimenez & Goding, 2019).

Gene expression analyses of melanoma cell lines and patient tumor biopsies led to the identification of two predominant

1 Department of Experimental Oncology, IEO, European Institute of Oncology IRCCS, Milan, Italy
2 Department of Surgery and Cancer, Imperial College London, London, UK
3 Department of Oncology and Hemato-oncology, University of Milan, Milan, Italy
4 Laboratory for Molecular Cancer Biology, Department of Oncology, KULeuven, Leuven, Belgium
5 Center for Cancer Biology, VIB, Leuven, Belgium
6 Laboratory for RNA Cancer Biology, Department of Oncology, KULeuven, Leuven, Belgium
7 Department of Biosciences, University of Milan, Milan, Italy
   *Corresponding author. Tel: +39 02 57489868; E-mail: piergiuseppe.pelicci@ieo.it
   **Corresponding author. Tel: +39 02 94375011; E-mail: luisa.lanfrancone@ieo.it
   †Present address: Institute of Oncology Research (IOR), Bellinzona, Switzerland
   ‡Present address: Candiolo Cancer Institute—FPO IRCCS, Candiolo Torino, Italy

EMBO reports   22: e50852 | 2021   **1 of 19**

transcriptional states, which are linked to phenotypically distinct cell populations, named, respectively, "proliferative" or "invasive" (Hoek *et al*, 2008). The proliferative phenotype is related to highly proliferating melanocytes and is characterized by the expression of *MITF*, the master transcription regulator of melanocyte proliferation and differentiation, and its upstream regulator *SOX10* (Bondurand *et al*, 2000; Lee *et al*, 2000; Potterf *et al*, 2000; Verastegui *et al*, 2000; Goding & Arnheiter, 2019). The invasive phenotype, instead, relates to an undifferentiated and highly invasive cell state that is under the control of a gene-regulatory network orchestrated by the AP1 and TEAD transcriptions factors (Riesenberg *et al*, 2015; Verfaillie *et al*, 2015). These undifferentiated/invasive melanoma cells are characterized by low levels of MITF and SOX10 and high levels of the tyrosine-protein kinase receptor AXL and ligands like TGFβ and WNT5A (Konieczkowski *et al*, 2014; Muller *et al*, 2014; Arozarena & Wellbrock, 2019). Of note, the proliferative and invasive phenotypes do not correlate with the presence of known driver mutations, including BRAF^{V600E} or NRAS^{Q61L}, indicating that transcriptional reprogramming is largely independent of the genetic make-up of individual tumor cells (Ferguson *et al*, 2017; Rambow *et al*, 2018).

These two phenotypic states are *per se* highly plastic and can convert into each others in response to changes in the TME, as revealed by the existence of single melanoma cells with transcriptional patterns consistent with transient phenotypic states (Tirosh *et al*, 2016b; Kim *et al*, 2017; Rambow *et al*, 2018; Arozarena & Wellbrock, 2019). A large body of experimental evidence indicates that the interconversion between the proliferative and invasive phenotypes play a major role during melanoma development ("phenotype-switch" model). In particular, the proliferative phenotype may drive tumor growth, and its transition into the invasive phenotype may generate cells able to invade and metastasize. Upon seeding at new sites, invasive cells must revert into a proliferative phenotype to allow metastasis growth (invasive-to-proliferative switch) (Carreira *et al*, 2006; Hoek *et al*, 2008; Pinner *et al*, 2009; Hoek & Goding, 2010; Rambow *et al*, 2018).

Phenotypic plasticity of melanoma cells also allows for adaptation to treatments and the emergence of resistant disease (Arozarena & Wellbrock, 2019; Rambow *et al*, 2019). Treatment with MAP-kinase inhibitors (MAPKi) has been associated with the progressive emergence of dedifferentiated cells that are intrinsically drug-resistant and possess transcriptional features of the invasive phenotype (expression of NGFR, PDGFR, IGF1R, EGFR, AXL, or ROR2) (O'Connell *et al*, 2013; Muller *et al*, 2014). On the other hand, melanomas that are resistant to checkpoint inhibitors express a similar transcriptional signature (innate anti-PD1 resistance signature; IPRES) that includes increased AXL expression (Hugo *et al*, 2016; Jenkins *et al*, 2018).

A proliferative-to-invasive phenotype switch, including resistance to targeted treatments, can be induced experimentally using some of the TME factors involved in melanoma progression, such as hypoxia, nutrient deprivation (glucose or glutamine), inflammation, TGFβ, WNT5A, or TNF-α (O'Connell *et al*, 2013; Widmer *et al*, 2013; Falletta *et al*, 2017; Arozarena & Wellbrock, 2019; Garcia-Jimenez & Goding, 2019; Vivas-Garcia *et al*, 2020). Instead, reversion of the invasive phenotype by manipulation of intracellular signaling pathway proved to be particularly difficult and successful approaches are still not known (Arozarena & Wellbrock, 2019).

Strikingly, using the zebrafish model system, it has been recently demonstrated that, after colonization of distant sites, invasive melanoma cells re-acquire a proliferative and differentiated phenotype, induced by the secretion of endothelins by the TME (Kim *et al*, 2017). These data suggest that the TME at distant sites provides the signals required to induce the invasive-to-proliferative switch, and targeting melanoma cell plasticity might represent an effective therapeutic option.

MITF seems to have a central, though controversial role in the modulation of plasticity and phenotype switches in melanoma (Goding & Arnheiter, 2019). However, changes in MITF expression in invasive cells do not induce the proliferative switch, suggesting that additional, yet poorly characterized, transcriptional changes are required for the maintenance of the invasive phenotype.

Over the past decade, long non-coding RNAs (lncRNAs) have been identified as critical players in gene regulation (Chen *et al*, 2018). They are defined as 5′-capped and 3′-polyadenylated RNA transcripts > 200 bp, with no or minimal protein-coding potential. Aberrant expression of lncRNAs is also associated to human tumorigenesis, including the process of metastasization (Huarte, 2015; Leucci *et al*, 2016a). In epithelial tumors, several lncRNAs (ATB21, HOTAIR, CHRF, Hh52) have been identified that regulate transcription factors (ZEB, SNAIL, TWIST) involved in the epithelial-to-mesenchymal transition (EMT), a process resembling the proliferative-to-invasive transition observed in melanomas (Gugnoni & Ciarrocchi, 2019). In melanoma, lncRNAs have been reported to promote survival (SAMMSON) (Leucci *et al*, 2016b), tumor suppression (Coe *et al*, 2019), growth or invasion (SPRY4-IT1, UCA1, MALAT-1, BANCR, PVT1, CASC15) of tumor cells (Lessard *et al*, 2015; Bhan *et al*, 2017).

However, whether lncRNAs contribute to establishment or maintenance of aberrant transcriptional patterns or phenotype plasticity in melanoma is unknown. We report here the identification of the TINCR lncRNA that acts as a suppressor of the invasive and metastatic phenotype in melanoma.

Results

Transcriptional profiles distinguish primary melanomas in two groups resembling nevi or metastases

To identify critical transcriptional-targets of metastatic dissemination, we performed unsupervised consensus clustering of 89 primary and 356 metastatic melanomas from The Cancer Genome Atlas (TCGA) and identified three stable clusters (Figs 1A and EV1A), none of which associated with NRAS or BRAF mutations (Fig EV1B). Primary melanomas were mainly distributed in Clusters 1 and 2 (~ 35 and ~ 56%, respectively; *P* < 0.01), while metastatic melanomas in Clusters 2 and 3 (~ 71 and ~ 22%, respectively; *P* < 0.01) (Fig 1A). Unsupervised consensus clustering of the 89 primary melanomas clearly identified two groups (Primary-A and Primary-B, Fig 1B), which corresponded to, respectively, Cluster 1 and Cluster 2/3 samples (31/34 of Primary-A were in Cluster 1; 54/55 of Primary-B in Clusters 2 or 3) (Fig EV1C). Differential expression analyses of Primary-A and Primary-B melanomas identified 1,034 genes (Primary Melanoma Signature; fold change ≥ 1.5, FDR ≤ 0.05) (Dataset EV1 and Fig EV1D). Down-regulated genes
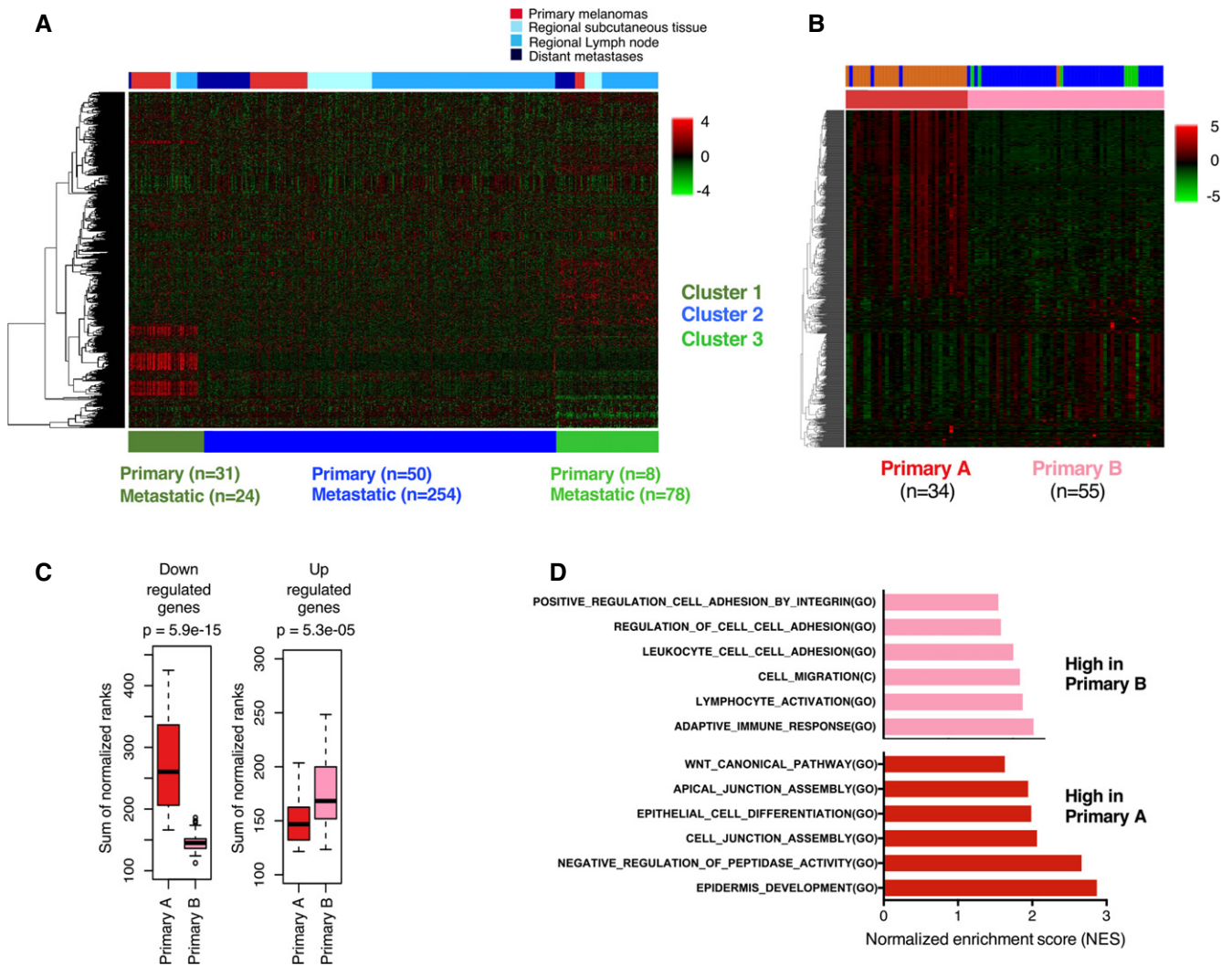
Figure 1. Unsupervised clustering of TCGA skin cutaneous melanoma RNA-seq dataset identifies two distinct groups of primary melanomas.

A Heatmap showing the unsupervised consensus clustering of TCGA melanomas (*n* = 445: 356 metastases and 89 primary melanomas). The identified clusters are indicated below the heatmap: cluster 1 (*n* = 55, red), cluster 2 (*n* = 304, blue), and cluster 3 (*n* = 86, green). Type of melanoma samples (primary or metastatic) and of metastatic site (subcutaneous, lymph node or distant) within each cluster are indicated below and above the heatmap, respectively.

B Heatmap showing the unsupervised consensus clustering of TCGA primary melanomas (*n* = 89) using the 1,000 most variable expressed genes in the same dataset. The identified signature clearly divides the TCGA dataset in two groups: Primary-A (*n* = 34, red) and Primary-B (*n* = 55, pink), as indicated.

C Boxplots showing the distributions of the normalized rank-sums of the down-regulated (left panel) and up-regulated (right panel) genes in the identified signature. Down-regulated genes in Primary-B melanomas better discriminate the two groups of primary melanoma samples (*P* = 5.9e-15, Wilcoxon rank-sum test). Median, minimum, maximum, 25th, 75th whiskers of rank-sum distribution are shown.

D Bar-graph showing the Gene Set Enrichment Analysis (GSEA) of genes differentially expressed between Primary-A and Primary-B melanomas (primary melanoma signature), performed combining GO gene sets (GO) and Gene set enrichment analysis (GSEA) of the primary melanoma signature.

prevailed over up-regulated for their power in discriminating the two groups (*P* = 5.9e-15 and 5.3e-05, respectively) (Fig 1C). The signature identified the same groups of Primary-A and Primary-B in an independent and larger dataset of 297 primary melanomas (Staaf *et al*, 2014; Fig EV2A) and in a small dataset of nevi and primary/metastatic melanomas from our tissue bank (12 samples, Fig EV2B). Notably, in the latter, Primary-A and Primary-B melanomas showed transcriptional similarity to nevi and metastatic melanomas, respectively (Fig EV2C and D; Spearman correlation coefficient ρ > 0.7).

Gene Set Enrichment Analysis (GSEA) of genes differentially expressed between Primary-A and Primary-B melanomas showed in Primary-B melanomas significant enrichment of genes involved in the regulation of immune responses and cell processes potentially relevant for the acquisition of the metastatic phenotype, including positive regulators of cell migration and integrin-mediated cell-cell adhesion, among others (Dataset EV2, Fig 1D). In Primary-A melanomas, instead, the most enriched processes were associated with epidermal and epithelial cell differentiation and a low invasive state (cell-cell and apical junction assembly), the WNT canonical

pathway, and the SOX10-driven transcriptional program (Dataset EV2, Fig 1D).

Together, these data indicate that primary melanomas can be grouped into two categories, based on their transcriptome similarities to nevi and metastatic melanoma, and that differences are consistent with the alternative enrichment of genes influencing cell differentiation (Primary-A; nevi-like) or invasive/migratory programs (Primary-B; metastasis-like), respectively.

TINCR lncRNA expression correlates with the non-metastatic phenotype

We then searched the primary melanoma signature for lncRNAs potentially implicated in the inhibition of the invasive switch in primary melanomas, e.g., expressed in Primary-A melanomas and down-regulated in Primary-B and metastases. We found three annotated lncRNAs in the signature, namely TINCR, KIAA0125 and MIAT. Only TINCR, however, was expressed in Primary-A melanomas and significantly down-regulated in Primary-B and metastatic melanomas (Mann–Whitney test, $P < 0.001$) (Fig 2A). TINCR RNA levels correlated significantly with the expression of down-regulated genes in the primary melanoma signature, as shown by the analyses of RNA-seq datasets of nevi ($n = 3$),

primary ($n = 4$) and metastatic melanomas ($n = 5$) (Spearman's correlation coefficient of 0.79, $P = 3.6e-3$) (Fig 2B). Down-regulation of TINCR in Primary-B melanomas was neither linked to variations in TINCR gene copy number (Fig EV3A), nor to hypermethylation of CpG dinucleotides flanking its transcription start site (TSS, Fig EV3B). QPCR analyses of primary and metastatic melanomas obtained from patient samples ($n = 8$ per group) or grown in immunodeficient mice (patient-derived xenografts; PDXs; $n = 4$, primary and $n = 8$, metastasis) showed lower levels of TINCR RNA in all metastatic samples (Fig 2C). Notably, matched pairs of PDXs from primary and metastatic samples of the same patient showed markedly reduced expression of TINCR in the metastatic counterparts (Fig 2C). Thus, TINCR RNA is expressed in Primary-A melanomas, whereas is down-regulated in Primary-B and metastatic samples, indicating that TINCR expression might contribute to the maintenance of the non-invasive phenotype.

TINCR silencing induces an invasive-phenotype switch

We next investigated the effects of TINCR silencing on the invasive phenotype of melanoma cells, focusing on cell migration/proliferation, tumorigenicity, drug sensitivity, and transcriptomic patterns.
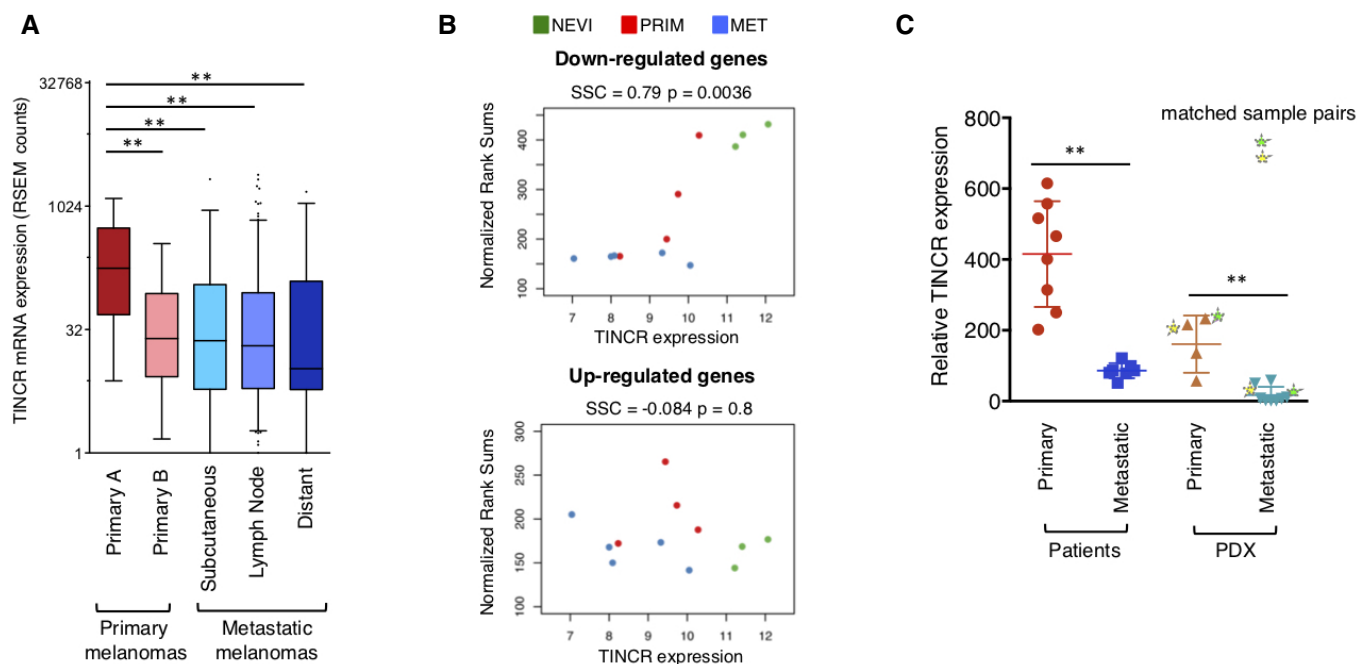

Figure 2. The lncRNA *TINCR* RNA is down-regulated in metastatic melanoma.

A Box and whiskers (from 5th to 95th percentile) plots depicting *TINCR* RNA levels in the TCGA SKCM RNA-seq dataset of melanoma samples. *TINCR* expression is higher in Primary-A melanomas, and its reduction in Primary-B melanomas and all groups of metastatic samples is statistically significant (Mann–Whitney test, **$P < 0.01$). Median, minimum, maximum, 25th, 75th whiskers of expression values are shown.

B Scatter plot showing correlation between the expression of *TINCR* RNA and normalized rank-sums of the down-regulated (upper panel) and up-regulated (lower panel) genes in the primary melanoma signature. *TINCR* expression strongly correlates (Spearman's correlation coefficient of 0.79, Spearman rank P value: **$P < 0.01$) with the expression of the down-regulated genes.

C Dot plot showing qRT–PCR analysis of *TINCR* expression in primary (8) and metastatic (8) melanoma samples from surgical specimens or patient-derived xenografts (4 primary and 8 metastatic PDXs). *TINCR* RNA levels relative to the L32P housekeeping gene are shown. Paired primary and metastatic PDXs are marked with an asterisk. The difference between primary and metastatic samples is significant (Mann–Whitney test, **$P < 0.01$). Median, minimum, maximum, 25th, 75th whiskers of expression values are shown.
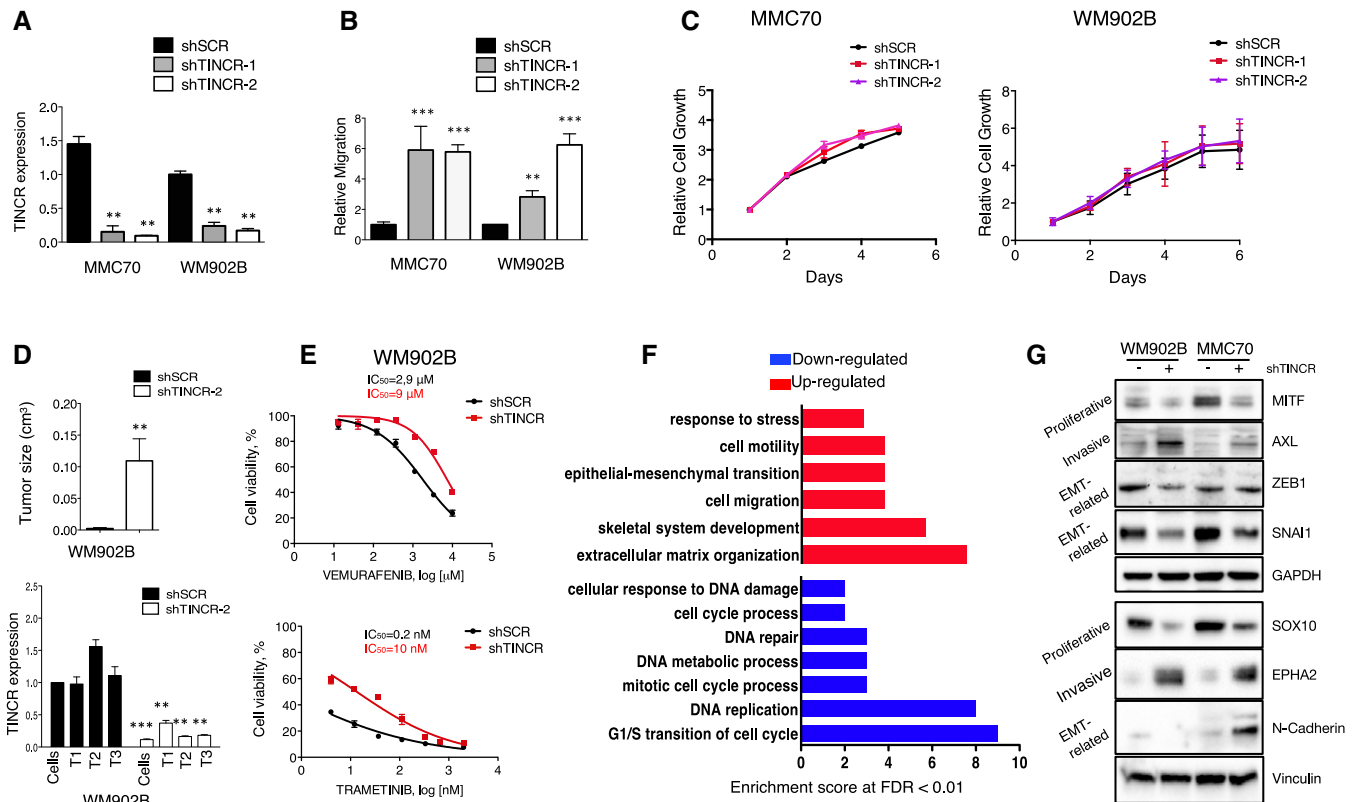
Figure 3. Loss of *TINCR* expression promotes melanoma cell migration *in vitro* and tumor growth *in vivo* by inducing a switch to an invasive phenotype.

A   qRT–PCR quantification of *TINCR* RNA expression in MMC70 and WM902B cell lines, independently infected with two shRNAs targeting *TINCR* expression (sh*TINCR*-1 and sh*TINCR*-2). Cells transduced with shScamble (shSCR) were used as control. *TINCR* RNA levels relative to L32P housekeeping gene and control (mean ± s.d.) measured in three independent biological experiments are shown. In both cell lines *TINCR* knockdown efficiency is more than 70% with the two shRNAs. Statistical analyses were performed using Student *t*-test (**$P < 0.01$).

B   *In vitro* migration assay of MMC70 and WM902B cells transduced with sh*TINCR*-1, sh*TINCR*-2, or shSCR. Relative migration (mean ± s.d.) from three independent experiments is indicated. Statistical analyses were performed using Student *t*-test (***$P < 0.001$).

C   *In vitro* cell proliferation of shSCR or sh*TINCR* infected MMC70 and WM902B cells assayed 72 h after infection at the indicated time points using *CellTiter-Glo* luminescent kit (Promega). Cell growth from three biological replicates is indicated as proliferation rate relative to control cells (mean ± s.d.). The difference between control and TINCR-silenced samples at all time points is not significant (Student *t*-test).

D   Upper panel: *in vivo* growth of tumors derived from intradermal injection of sh*TINCR*-2 or shSCR WM902B cells in NSG mice. 600,000 WM902B cells per mouse were inoculated. Tumor volumes (mean ± s.d.) were measured 8 weeks after transplantation. Results from two independent experiments (four animals per group) are shown. Statistical analysis between control and *TINCR*-silenced groups was performed using the Student *t*-test (**$P < 0.01$). Lower panel: qRT–PCR analysis of *TINCR* RNA expression in tumors derived from *in vivo* transplant of shSCR and sh*TINCR* WM902B cells (8 weeks after injection). *TINCR* RNA levels relative to L32P housekeeping gene and control (mean ± s.d.) from four biological replicates (animals) from both experiments are shown.

E   Drug-response curves showing increased resistance of sh*TINCR*-WM902B cells after treatment with BRAF (Vemurafenib; from 10 to 10,000 nM) and MEK (Trametinib; from 4 to 2,000 nM) inhibitors. The shSCR- (control) and sh*TINCR*-WM902B cells were treated with increasing concentrations of drugs and their viability assayed after 72 h using *CellTiter-Glo* luminescent kit (Promega). Error bars represent s.e.m. of three biological replicates. The dose-response curve was fit with nonlinear regression (GraphPad Prism).

F   Gene ontology (GO) terms enrichment analysis of the differentially expressed genes identified by RNA-seq analysis in *TINCR* knockdown WM902B cells. All enrichments are significant at FDR < 0.05.

G   Western blot analysis of a panel of proteins that are specifically associated to the proliferative or invasive phenotype. Total protein lysates were extracted from shSCR- and sh*TINCR*-WM902B cells (lane 1 and 2) or shSCR- and sh*TINCR*-MMC70 cells (lane 3 and 4) 10 days after infection and analyzed by immunoblot assay using the indicated antibodies. Vinculin was used as loading control.

We used two melanoma cell lines (WM902B and MMC70) with relatively high levels of TINCR RNA (Figs 3A and EV3C), and expressing a proliferative, non-invasive phenotype (as shown by high levels of MITF and SOX10 proteins and low of AXL and EPHA2, respectively) (Fig 3G). Infection with lentiviral vectors carrying TINCR-specific (shTINCR-1 and shTINCR-2) shRNAs reduced significantly TINCR RNA levels (> 75%), as compared to control (shSCR) shRNAs (Fig 3A).

In vitro migration was significantly increased in both WM902B and MMC70 cells by TINCR knockdown (Figs 3B and EV3D). As well, TINCR-depleted WM902B cells showed increased capacity to invade the collagen matrix in a 3D collagen assay (Fig EV3E). Proliferation, instead, was not affected in either of the two cell lines (Fig 3C). Analyses of *in vivo* tumor growth (WM902B cell line) showed a dramatic increase in the size of tumors obtained upon

intradermal injection of shTINCR cells, as compared to shSCR control cells (Fig 3D, upper panel). Notably, shTINCR tumors showed very low levels of TINCR RNA, even at long time points after injection (8 weeks) (Fig 3D, lower panel, and Dataset EV3A).

To investigate the effects of TINCR expression on drug sensitivity, TINCR-depleted WM902B cells were treated with the BRAF PLX4032 (Vemurafenib) and MEK GSK1120212 (Trametinib) inhibitors. WM902B cells carry the BRAF^{V600E} mutation and are sensitive to both BRAF and MEK inhibition (Zipser et al, 2011). Analyses of cell viability at 72 h showed increased resistance of shTINCR-WM902B cells to both drugs, as compared to control shSCR cells (Fig 3E).

RNA-seq analysis of the changes in global RNA abundance in TINCR-silenced WM902B cells showed significant modulation of the expression of 1,117 genes (fold change > 1.5, FDR < 0.05; 637 up- and 480 down-regulated) (Fig EV4A and Dataset EV3B). In TINCR-depleted cells, GSEA and Gene Ontology (GO) analyses showed enrichment of genes involved in the regulation of invasion and metastasis (extracellular matrix organization, cell motility/migration, EMT, and the invasive melanoma signature) and depletion of genes involved in proliferation (cell cycle; DNA replication and the proliferative melanoma signature) (Figs 3F and EV4B). Consistently, attenuation of TINCR expression induced marked up-regulation of AXL and EPHA2 proteins and concomitant down-regulation of MITF and SOX10 proteins, markers of the proliferative cell state involved in the regulation of melanocytic lineage-identity and survival (Fig 3G). TINCR silencing also modulated expression of several EMT-related markers, including N-cadherin, SNAI1, and ZEB1 (Fig 3G), which have been implicated in the regulation of cell plasticity, phenotypic heterogeneity and drug resistance (Vandamme & Berx, 2014). As well, silencing of TINCR expression in the growing WM902B tumors induced enrichment or depletion, respectively, of genes of the invasive or proliferative signatures (Fig EV4C). Together, these data demonstrate that TINCR silencing induces a switch toward the invasive phenotype without affecting cell proliferation, indicating that TINCR expression maintains melanoma cells in a non-invasive state. Notably, down-regulation of TINCR expression in an invasive melanoma cell line with high levels of TINCR (WM1552C; Figs EV3C and EV4D, upper panel) and undetectable levels of MITF and SOX10 (Fig EV4D, lower panel), further increased expression of invasive markers (AXL, EGFR, and EPHA2 proteins) (Fig EV4D, lower panel), in vitro cell migration and tumor formation in vivo (Figs EV4E, upper panel and EV4F), without exerting significant effects on cell proliferation in vitro (Fig EV4E, lower panel), suggesting that TINCR limits the expression of the invasive phenotype irrespective of the status of MITF expression.

Finally, we investigated if MITF is involved in the maintenance of TINCR expression in proliferative phenotype melanoma cells. Publicly available chromatin immunoprecipitation analyses, in fact, reported several MITF-binding sites variably present in different melanoma cell lines (at +28.6, +3.8 and +0.36 Kb from its TSS) (Webster et al, 2014; Laurette et al, 2015; Johansson et al, 2020; Louphrasitthiphol et al, 2020). TINCR RNA levels are reduced upon MITF depletion in WM902B and MMC70 cells, suggesting that steady-state levels of TINCR depend on MITF expression (Fig EV5A).

TINCR re-expression in metastatic melanoma reverts the invasive phenotype

We next investigated whether restoration of TINCR expression reverts the invasive phenotype, using two PDXs from metastatic melanomas expressing low levels of TINCR RNA (Fig 2C) and carrying, respectively, NRAS (N61L; MM13 PDX) or BRAF mutations (V600E; MM2 PDX). Infection of cell suspensions from PDX-derived tumors using lentiviruses carrying empty vector or TINCR full-length cDNA lead to ~ 8-fold increase of TINCR expression in both PDX samples, as evaluated by qPCR at 72 h post-infection (Fig 4A).

TINCR overexpression (i) markedly reduced cell migration in vitro (~ 75 and ~ 65% reduction for MM13 and MM2 cells, respectively) (Figs 4B and EV5B); (ii) significantly reduced invasion capacity of MM2 spheroids in collagen (Fig EV5C); (iii) exerted no significant effect on cell proliferation (Fig 4C); (iv) increased in vitro drug sensitivity to the MEK inhibitor Trametinib in MM13 and MM2 PDX cells, and to the BRAF inhibitor Vemurafenib in MM2 cells (Fig 4D). We performed global RNA-seq analyses of TINCR-overexpressing MM13 and MM2 cells (Dataset EV4A and B; common genes reported in Dataset EV4C). GSEA identified enrichment in translation and RNA metabolism, cell division, and cell-cell and cell-matrix communication (Dataset EV4D–G). Matching DEGs from TINCR-overexpresing cells with those of WM902B tumors (Fig EV4C, Dataset EV3A) and cells (Fig 3F, Dataset EV3B) showed 238 and 257 common genes, in MM2 and MM13, respectively, with a relatively low number of inverted changes (84 and 70, respectively; now reported in Datasets EV3 and EV4), which mapped to GO terms associated to cell-matrix adhesion, migration and motility. Consistently, TINCR-overexpressing cells showed down-regulation of a set of genes belonging to the invasive signature, and up-regulation of genes of the proliferative signature (Fig EV5D, Dataset EV4). Western blot analysis of the same samples revealed a significant reduction of the expression of the invasive markers: EPHA2 and EGFR in both MM13 and MM2; AXL and PDGFRβ in MM13 and MM2, respectively. The SOX10 proliferative marker was up-regulated in MM2, while was not expressed in MM13. Notably, analyses of MITF expression in MM2 and MM13 cells, as well in cells from other two PDXs (MM3 and MM19), increased MITF expression in only one PDX (MM2) and had variable effects on the others, suggesting that the effect of TINCR overexpression on MITF is cell-context dependent (Figs 4E and EV5E).

Thus, re-expression of TINCR in metastatic melanoma cells restrained cell migration and expression of critical markers of the invasive state and restored drug sensitivity, with no effects on cell proliferation.

To analyze the effect of TINCR overexpression on in vivo tumorigenicity, control and TINCR-overexpressing MM13 PDX cells were injected orthotopically in NSG mice, and, after 30 days, primary tumors resected surgically. Tumors removed from the TINCR-overexpressing group were significantly smaller than those from the control group (P < 0.01; Fig 4F). One month after resection, control animals developed spontaneous metastases to lung, liver, and lymph nodes (LN), while, in the TINCR-overexpressing mice, metastasis formation was almost
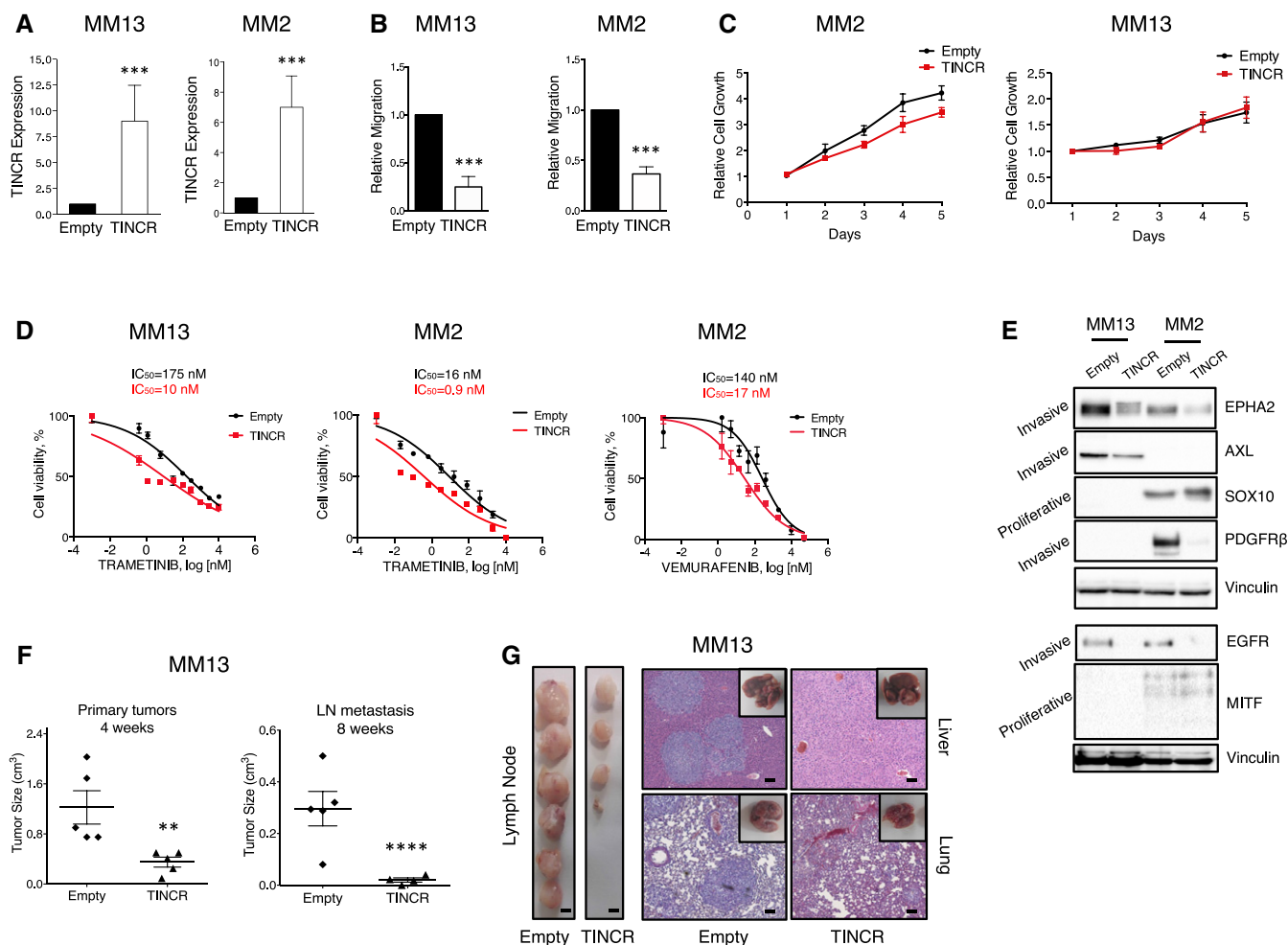
Figure 4. TINCR re-expression inhibits migration *in vitro*, tumor growth, and metastasis spreading *in vivo* and overcomes resistance to MEK inhibitors of metastatic melanoma PDXs.

A   qRT–PCR analysis of *TINCR* expression (left) of MM13 and MM2 PDX cells infected with lentiviral vectors expressing full-length *TINCR* cDNA. PDX cells infected with empty vector (Empty) were used as control. *TINCR* RNA levels relative to L32P housekeeping gene and control (mean ± s.d.) from three biological replicates are shown. Statistical analyses were performed using Student *t*-test (***$P < 0.001$).

B   *In vitro* relative migration (mean ± s.d.) from three independent experiments (biological replicates) is shown in MM13 and MM2 *TINCR*-overexpressing (*TINCR*) compared to control (Empty) cells. Statistical analyses were performed using Student *t*-test (***$P < 0.001$).

C   *In vitro* cell proliferation was assayed 72 h post-infection in Empty and *TINCR* MM13 and MM2 PDX cells at the indicated time points (1–5 days) using *CellTiter-Glo* viability assay. Relative proliferation rate (mean ± s.d.) of three independent experiments are shown.

D   Drug-response curves showing sensitization to MEK inhibitor Trametinib of MM13 (NRAS-mutant PDX) and to Trametinib and BRAF inhibitor Vemurafenib of *TINCR* MM2 cells (BRAF-mutant PDX). The Empty (control) and *TINCR* expressing MM13 cells were treated with increasing concentrations of drug (ranging from 5 to 5,000 nM) and cell viability was assayed after 72 h by *CellTiter-Glo* viability assay. Error bars represent s.e.m. of three biological replicates. The dose-response curve was fit with nonlinear regression (GraphPad Prism).

E   Western blot analysis of the expression of the invasive and proliferative phenotype markers EPHA2, EGFR, AXL, PDGFRβ, SOX10, and MITF in *TINCR*-overexpressing MM13 and MM2 cells. Total protein lysates were extracted from PDX cells 7 days after infection and analyzed by immunoblot assay using the indicated antibodies. Vinculin was used as loading control. This experiment is representative of three independent experiments showing comparable levels of *TINCR* overexpression (8–10 folds).

F   *In vivo* growth of Empty vector and *TINCR* cDNA expressing MM13 cells following intradermal injection into NSG mice. Four animals (200,000 cells/mouse) per group were used in each experiment. Tumor growth (mean ± s.d.) was monitored weekly and tumor volume (mean ± s.d.) measured at 4 weeks for primary tumors (originated in the site of injection, left panel) and at 8 weeks for spontaneous metastases which colonized lymph nodes (right panel). The results of two independent experiments are shown. Statistical analyses of control and TINCR-overexpressing groups from both experiments were performed using Student *t*-test (**$P < 0.01$).

G   Representative pictures of lymph node metastases derived from Empty and *TINCR* expressing MM13 PDX cells are shown. Hematoxylin-eosin staining of sections of liver and lung metastases derived from Empty and *TINCR* MM13 PDX cells. Metastasis formation was evaluated 8 weeks after transplantation into NSG mice. Pictures of representative lungs and livers infiltrated with metastases are shown in the inset. Scale bars: 200 μm.

abolished at LN sites and significantly reduced in lung and liver (Fig 4F and G).

To investigate cellular mechanisms of reduced tumorigenicity in TINCR-overexpressing PDXs, we analyzed the frequency of proliferating, apoptotic and tumor-initiating (TIC) cells *in vivo*. We found comparable levels of proliferating (measured as Ki67- or phospho S10 Histone H3-positive cells) and apoptotic (measured as cleaved caspase3-positive cells) cells in tumors obtained from orthotopic injection of control and TINCR-overexpressing cells (Fig EV5F; same tumors as in Fig 4F). To determine the TIC frequency, we performed extreme limiting dilution assays (ELDA) (Hu & Smyth, 2009) of control and TINCR-overexpressing MM13 PDX cells and measured

tumor development. Notably, TINCR-overexpressing cells showed reduced frequencies of tumor-initiating capacity *in vivo* (2–3 fold), as compared to control cells ($P = 0.047$; Fig EV5G), suggesting that TINCR expression regulates numbers of TICs and that this contributes to the reduced tumorigenicity of *TINCR*-overexpressing melanoma cells.

Together, these data indicate that restoration of TINCR expression reverts the invasive melanoma phenotype of metastatic melanoma, as shown by its effects on cell migration, expression of invasive markers, resistance to MEK and BRAF inhibitors, and, *in vivo*, frequency of tumor-initiating cells, tumor growth, and metastatic potential.
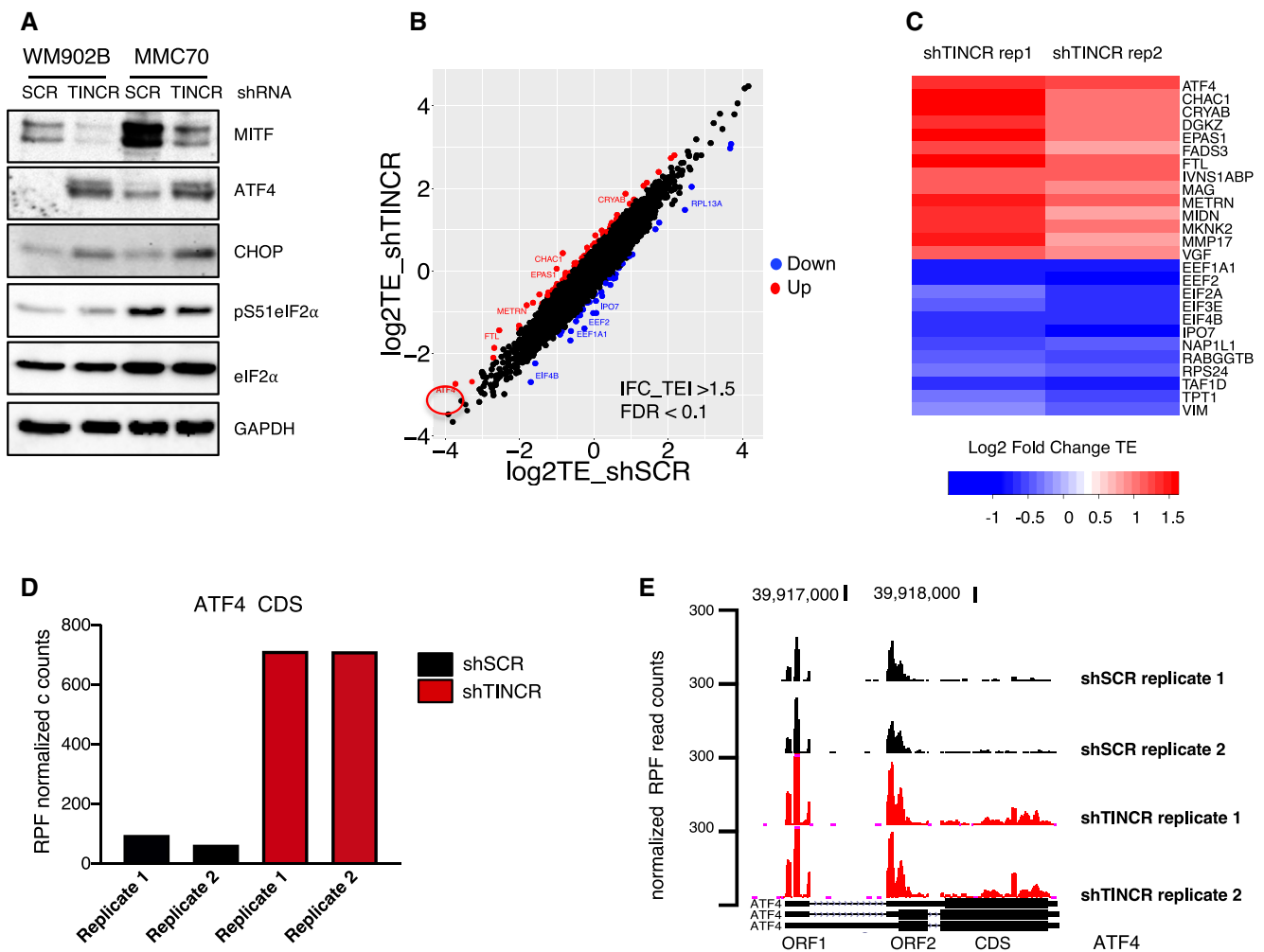

Figure 5. TINCR depletion activates ATF4 translation independently of eIF2α phosphorylation.

A   Western blot analysis of integrated stress response activation in WM902B and MMC70 cells. Cells were harvested 96 h after shRNA infection and Western blot performed using the indicated antibodies.

B   Representative comparison of translational efficiency (TE) in control (shSCR) and sh*TINCR* WM902B cells 72 h post-infection. The genes with statistically significant TE up- and down-regulation (FDR < 0.1) are highlighted in red and blue, respectively. ATF4 is circled among the up-regulated genes.

C   Heatmap representing top translationally up-regulated and down-regulated genes in *TINCR* WM902B cells. The plotted values are the log2 fold TE change values in each biological replicate (rep1 and rep2) relative to control (shSCR).

D   Bar-graph representing ribosome-protected fragments (RPF) normalized coverage (mean ± s.d.) mapping to ATF4 CDS in control (shSCR) and *TINCR* (sh*TINCR*) depleted WM902B cells from two biological replicates is shown.

E   UCSC genome browser tracks of ribosome footprint data illustrating RPF density distribution across ATF4 mRNA in shSCR and sh*TINCR* WM902B cells.

TINCR depletion induces ATF4 up-regulation and MITF down-regulation in the absence of a typical integrated stress response

We next investigated the molecular mechanisms underlying the invasive-phenotype switch induced by TINCR silencing. In melanoma, invasion correlates with low expression of MITF, a key regulator of the melanocyte lineage that promotes survival, induces proliferation and maintains the differentiated phenotype (Goding & Arnheiter, 2019). As a consequence, MITF-low cells are slow-cycling, invasive, and endowed with melanoma-initiating cell properties (Carreira et al, 2006; Goodall et al, 2008; Cheli et al, 2011). Down-regulation of MITF during the proliferative-to-invasive switch is mediated by inhibition of both translation, through the eukaryotic translation initiation factor eIF2α or the RNA helicase DDX3X (Phung et al, 2019), and transcription, through the POU domain transcription factor Brn-2 or the activating transcription factor 4 (ATF4) (Goodall et al, 2008; Falletta et al, 2017). ATF4 is a controller of the integrated stress response (ISR), which is induced in melanoma cells by nutrient starvation and inhibition of eIF2 (Falletta et al, 2017; Ferguson et al, 2017; Garcia-Jimenez & Goding, 2019). Strikingly, Western blotting of shTINCR WM902B and MMC70 melanoma cells showed marked down-regulation of MITF and increased expression of ATF4 and its transcriptional target CHOP (DDIT3), as compared to control cells (Fig 5A). Consistently, MITF and ATF4 target genes were, respectively, depleted and enriched in the transcriptome of shTINCR WM902B cells (Appendix Fig S1A).

To investigate the functional role of ATF4 activation following TINCR depletion, we down-regulated ATF4 expression in WM902B and MMC70 melanoma cells, using ATF4-specific shRNAs (Appendix Fig S1B). ATF4 silencing had no significant effects on cell migration of either WM902B or MMC70 melanoma cells; it rescued, however, the increased migratory phenotype induced by TINCR depletion (Appendix Figs S1C and D), suggesting that ATF4 is critical for the phenotype switch induced by TINCR. We also noticed that down-regulation of MITF by shTINCR is maintained upon simultaneous silencing of ATF4 (Appendix Fig S1B), suggesting that TINCR-induced MITF down-regulation is not linked to ATF4 activation.

We next investigated mechanisms underlying ATF4 activation following TINCR depletion. Induction of ATF4 requires phosphorylation of eIF2α, a common substrate of the different stress-kinases that initiate the ISR (Wek & Cavener, 2007; Pakos-Zebrucka et al, 2016). Phosphorylated eIF2α reduces the formation of the translation initiation eIF2-GTP-tRNAi(Met) ternary complex (TC) (Kedersha et al, 2002), leading to a suppression of global protein synthesis and the selective translation of a specific mRNA subset of stress proteins, including ATF4 (Pakos-Zebrucka et al, 2016; Pavitt, 2018). Surprisingly, however, we did not observe any modification in phosphorylation of eIF2α upon TINCR knockdown in either MITF-positive WM902B and MMC70 or MITF-negative WM1552C melanoma cells (Fig 5A and Appendix Fig S2A). To exclude a transient effect of shTINCR on eIF2a phosphorylation, we performed a time course experiment on cells transfected with TINCR siRNAs, which showed ATF4 up-regulation at 8 h post-transfection, in the absence of any changes in eIF2a phosphorylation (Appendix Fig S2B). Thus, TINCR RNA depletion induces the ATF4-high cellular state typical of invasive melanoma cells, in the absence, however, of eIF2B inhibition,

suggesting that TINCR regulates ATF4 through mechanisms that are independent of its canonical induction by cellular stresses.

ATF4 translation can be induced independently of ISR by the rapamycin complex 1 (mTORC1), a protein kinase complex that activates protein synthesis in nutrient-rich conditions, and promotes cellular growth (Nandagopal & Roux, 2015; Saxton & Sabatini, 2017). mTORC1 phosphorylates the S6 kinase (S6K) and the translation initiation factor 4E (eIF4E)-binding protein 1 (4EBP1), which induces its release from eIF4E to stimulate cap-dependent translation (Qin et al, 2016). Upon TINCR depletion, levels of phosphorylated S6K and 4EBP1 decreased slightly in WM902B but not MMC70 cells, suggesting that ATF4 induction by TINCR depletion is independent on mTORC1 pathway activity (Appendix Fig S2B).

TINCR depletion induces translational reprogramming and increases protein synthesis

We then investigated alternative mechanisms of ATF4 regulation by TINCR. Several ATF4-regulatory mechanisms were previously reported, including increased transcription and protein stability (Wortel et al, 2017). ATF4 mRNA is not regulated by TINCR, as shown by analyses of the transcriptome of shTINCR WM902B (Dataset EV5), and confirmed by PCR analyses of both WM902B and MMC70 cells (Appendix Fig S2C, upper panel). As well, ATF4 protein showed similar half-life in TINCR-depleted WM902B and MMC70 cells upon treatment with the protein synthesis inhibitor cycloheximide, suggesting that TINCR does not regulate ATF4 protein stability in melanoma cells (Appendix Fig S2C, lower panel).

In the ISR, ATF4 is induced by de novo protein synthesis (mRNA translation), in response to phosphorylation of eIF2α (Pakos-Zebrucka et al, 2016). To investigate whether TINCR regulates ATF4 mRNA translation, we measured genome-wide translation via deep sequencing of mRNA fragments bound by 80S translating ribosomes (Ribo-seq) in WM902B cells (Ingolia et al, 2019). We identified 97 mRNAs whose translational efficiency (TE) was significantly altered (57 with increased and 40 with decreased TE; FC > 1.5, FDR < 0.1) (Dataset EV5). Notably, ATF4 scored among the top up-regulated mRNAs (Dataset EV5 and Fig 5B). ATF4 and the other two top translationally induced mRNAs—CHAC1 and EPAS1—showed increased protein levels in WM902B cells upon transduction with two different TINCR shRNAs (Appendix Fig S2D). Analyses of the other mRNAs with increased TE revealed enrichment of several transcripts encoding other proteins involved in the ISR (e.g., EPAS1/HIF2α, CHAC1, FTL) (Fig 5B and C). Thus, TINCR depletion induces translational reprogramming, leading to increased translation of ATF4 and other ISR proteins.

The mature ATF4 transcript contains two short and alternative upstream ORFs (uORF1-2). Under steady-state conditions, the leaky ribosome-scanning of ORF1 allows re-initiation at the start codon of uORF2, thus suppressing translation of the ATF coding sequence (CDS). During ISR, the ATF4 CDS is actively translated as a consequence of leaky scanning of ORF2 and start codon selection, due, respectively, to limiting concentrations of the TC complex and regulation of mRNA methylation (m6A) in the 5′ UTR (Zhou et al, 2018). In control WM902B melanoma cells, Ribo-seq showed only background levels of ribosome density across the main ATF4 CDS, while displaying a considerable amount of footprints in uORFs 1 and 2. In TINCR-depleted cells, a significant amount of footprints

appeared instead in the main CDS, consistently with the increased translation of ATF4 (Fig 5D and E). ORF1 and ORF2, however, did not show any decrease of ribosome footprint (Fig 5E), reinforcing the conclusion that TINCR regulates ATF4 translation through mechanisms that are independent of eIF2α phosphorylation.

To investigate alternative mechanisms of activation of ATF4 translation by TINCR depletion, we analyzed the effects of TINCR knockdown on translation elongation, a key regulatory step for translational control, which is attenuated under conditions of nutrient and energy depletion (Knight et al, 2020). Central to this process is the eukaryotic elongation factor 2 (EEF2) kinase, which is activated by stress and phosphorylates EE2F, leading to attenuation of translation elongation (Proud, 2015) and selective translation of TOP (terminal oligopyrimidine) mRNAs, a family of transcripts that regulates translation, that is translationally repressed following serum, aminoacid or oxygen deprivation (Meyuhas & Kahan, 2015), and encodes several ribosomal proteins, all five elongation factors (1A, 1B2, 1D, 1G, 2), and three subunits the eIF3 functional core (eIF3e, eIF3f and eIF3h) (Pichon et al, 2012; Meyuhas & Kahan, 2015).

Western blotting of TINCR-depleted WM902B and MMC70 cells showed significantly decreased levels of phosphorylated EEF2 (Appendix Fig S2E). Analyses of de novo protein synthesis in the same cells by 35S-methionine labeling showed increased global protein synthesis (Appendix Figs S2F and G). Analyses of the top 40 mRNAs with decreased TE in the Ribo-seq profiling of TINCR-depleted RNAs (Dataset EV5) revealed enrichment of a subset of the TOP mRNAs, including transcripts encoding ribosomal proteins (RPL4, RPL5, RPL13A, RPL28, RPS24), initiation factors (EIF4B, EIF3E, EIF2A, EIF3L, EIF3F, EIF2S3, EIF3H) and, most notably, key regulators of elongation (EEF2, EEF1A1, EEF1B2), whose downregulation might significantly reduce elongation kinetics (including that of uORFs), and affect the process of re-initiation. These data suggest that TINCR depletion increases translation elongation and general protein synthesis, and induces translational reprogramming of specific mRNAs, leading to increased translation of TOP mRNAs, ATF4, and other proteins involved in the ISR.

TINCR interacts with ISR RNAs and represses their translation

To investigate how TINCR regulates translational reprogramming, we mapped TINCR–RNA interactions by RNA interactome analyses and deep sequencing (RIA-seq) (Kretz et al, 2013). To this end, 20 antisense oligonucleotide probes spanning the entire length of the TINCR transcript were pooled in two sets (based on their relative sequence positions, odd and even) (Fig 6A), biotinylated at their 5′ end, and used to pulldown the endogenous TINCR RNA and its RNA interactors from glutaraldehyde-fixed WM902B and MMC70 cells. As controls, we used an equal number of scrambled oligonucleotide probes (SCR). QPCR analysis confirmed the enrichment (10–20 fold) of TINCR RNA in pulldown experiments from both cell lines (Fig 6B). mRNA libraries from TINCR "odd" and "even" pulldowns were then sequenced and aligned to the human genome scaffold. Only peaks enriched in both "even" and "odd" samples, as compared to input, were considered for further analysis. We identified 198 peaks in common between WM902B and MMC70 cells, mapping to 142 genes (Dataset EV6, Appendix Figs S3A and B). More than 90% of the TINCR-bound RNA fragments mapped to

gene bodies, with only ~ 10–20% mapping within introns (Appendix Fig S3C). Notably, among the top-enriched TINCR-interacting mRNAs (by both peak number and fold enrichment; Dataset EV6), we identified ATF4 (Fig 6C, Dataset EV6). Enrichment of the ATF4 mRNA was also validated by qRT–PCR in both WM902B and MMC70 cells (Fig 6B, right panel). GSEA analysis showed that TINCR interactome was enriched in mRNAs involved in response to stress, cell death, proteolysis and others (Fig 6D). Among the other TINCR-interacting mRNAs, we identified several transcripts encoding other proteins of the ISR, including SOGA1, HSP90B2P, CHAC1, and IER2 (Dataset EV6, Appendix Fig S3A).

Analyses of their primary sequence suggests direct interactions between TINCR and TINCR-interacting RNAs. De novo RNA-binding motif enrichment analyses identified a 10 nt RNA-binding motif strongly enriched in 25 TINCR-interacting transcripts, including ATF4 and TINCR itself (Appendix Figs S4A and B). A thermodynamics prediction algorithm identified the ATF4-TINCR interaction site, which contains or is adjacent to the ATF4 or TINCR binding motifs, respectively (Appendix Fig S4C). Alternatively, TINCR may regulate ATF4 translation indirectly, by sequestering specific miRNAs that negatively regulates ATF4 (mir-1283 e mir-214) (Wang et al, 2013; He et al, 2016; Gao et al, 2016; McMahon et al, 2017). Notably, we found mir-1283 in the TINCR-specific pulldowns from WM902B cells (Appendix Fig S5A).

Next, we investigated the overlap between TINCR-interacting mRNAs ($n = 2,158$; from the RIA-seq dataset) and mRNAs that are transcriptionally ($n = 1,117$; from the RNA-seq dataset) or translationally ($n = 97$; from the Ribo-seq dataset) regulated by TINCR in WM902B cells. In the TINCR interactome, we found 13% ($n = 154$) of the transcriptionally regulated and 46% ($n = 45$) of the differentially translated mRNAs (Appendix Fig S5B, Dataset EV7). Notably, 40 of the 45 differentially translated and TINCR-interacting mRNAs (~ 90%) were translationally up-regulated in TINCR-silenced melanoma cells, suggesting that physical interaction of TINCR with target mRNAs reduces their translational efficiency (Dataset EV7).

Together, these data demonstrate that TINCR interacts with a specific subset of mRNAs, including ATF4 and other ISR proteins and regulators of translation, reducing their translational efficiency, suggesting that the effect of TINCR on gene expression regulation is mainly due to mRNA-binding and regulation of translation, rather than regulation of global mRNA turnover or transcription. Consistently, single molecule fluorescent in vitro hybridization (FISH) showed that TINCR lncRNA is almost exclusively localized in the cytoplasm in melanoma cells (Appendix Fig S5C), as previously reported for other cell types (Kretz et al, 2013).

Discussion

We identified TINCR as one component of the transcriptional signature that distinguishes primary melanomas in two groups, nevi- or metastasis-like, and is enriched of invasion/migration genes. TINCR expression is significantly higher in nevi-like primary melanomas, suggesting that it contributes to the maintenance of the non-invasive phenotype. Accordingly, TINCR silencing induced the invasive phenotype in proliferative phenotype melanoma cell lines, as defined by the appearance of typical markers of invasiveness (high AXL and high EPHA2; low MITF and low SOX10; modulation of the
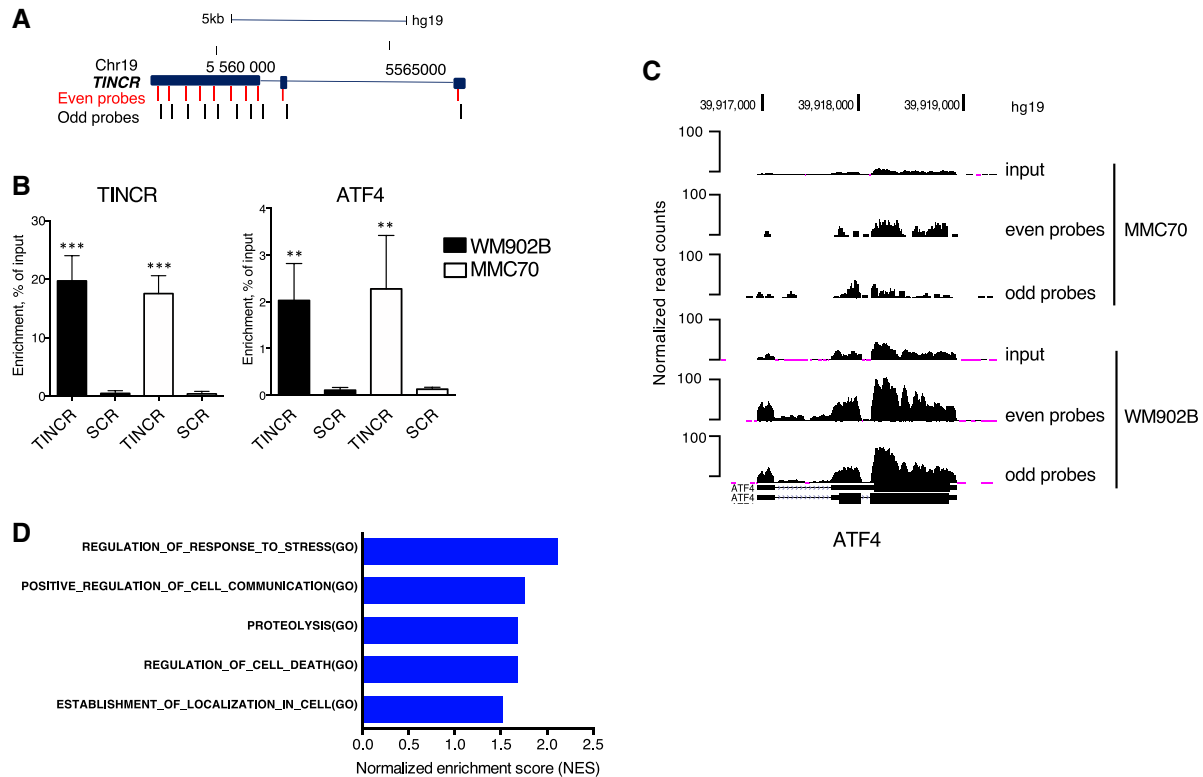
Figure 6. Identification of *TINCR*-interacting mRNAs through *TINCR* interactome analysis (RIA-seq).

A Schematic representation of biotinylated antisense DNA probes complementary to *TINCR* transcript. Odd (black) and even (red) probes were used for RNA pulldown.

B QPCR validation of *TINCR* and *ATF4* RNA recovery in *TINCR* antisense pulldown. Enrichment relative to input (mean ± s.d.) from three independent pulldown experiments is shown. Statistical analyses were performed using Student *t*-test (**P < 0.01, ***P < 0.001).

C UCSC genome browser tracks of *TINCR*–RIA-seq sequencing reads illustrating coverage and enrichment across ATF4 transcript in WM902B and MMC70 cells.

D Gene set Enrichment analysis (GSEA) of *TINCR*-interacting RNAs (FDR < 0.25) using Gene Ontology (GO) database.

N-cadherin, SNAIL, and ZEB1) and increased *in vitro* cell migratory properties. Most notably, re-expression of TINCR in melanomas with low levels of TINCR induced down-regulation of the invasive gene signature, as well as reduction of the corresponding markers (PDGFRβ, AXL, EPHA2 and EGFR), *in vitro* cell migration and *in vivo* metastatic potential, suggesting that TINCR overexpression reverts the invasive phenotype.

The capacity of TINCR overexpression to revert the invasive phenotype is remarkable. While many experimental models are available to induce the proliferative-to-invasive switch (Hoek & Goding, 2010), inducing the invasive-to-proliferative switch is difficult to obtain experimentally (Arozarena & Wellbrock, 2019). Single-Cell RNA-seq analyses of individual melanoma cells revealed the co-existence of cells with either proliferative or invasive phenotypes (MITF-high or MITF low) and, remarkably, of cells with intermediate phenotypes, suggesting the existence of transient cell states between the proliferative and invasive phenotypes (Ennen *et al*, 2015; Tirosh *et al*, 2016a). Prolonged exposure to specific environmental signals, such as nutrient limitation or therapies, converts the transient transcriptional states to stably invasive and drug-resistant states, by fixing specific transcriptional patterns via global epigenetic reprogramming (Garcia-Jimenez & Goding, 2019). Likewise, specific environmental

signals may induce the fixation of the non-invasive phenotype. Emerging evidence indicates that the reversion of the invasive phenotype is the consequence of the integration of different environmental signals at the metastatic sites, which are, however, only partially known (Arozarena & Wellbrock, 2019). Notably, the genes of the invasive signature that are down-regulated upon TINCR overexpression in metastatic melanomas are highly enriched for target genes of the TEAD transcription factors (Appendix Fig S5D). TEADs have been recently shown to be critical for the establishment of the epigenetic landscape associated with invasive transcriptional patterns, and by themselves necessary to maintain the invasive phenotype (Verfaillie *et al*, 2015). Thus, TINCR might regulate signaling and/or transcriptional pathways that are implicated in the establishment of the chromatin of the invasive state.

Modulation of TINCR expression also influenced the sensitivity of melanoma cells to targeted drugs. The acquisition of resistance to targeted drugs seems to be due to increased expression of the AXL tyrosine-kinase (Muller *et al*, 2014; Boshuizen *et al*, 2018) and is associated with the emergence of MITF-low/AXL-high melanoma cells (Sensi *et al*, 2011; Kozar *et al*, 2019). Notably, attenuation of TINCR expression in melanoma cells induced enrichment of the AXL-high transcriptional program (Appendix Fig S5E, left panel),

while its overexpression reduced expression of several receptor tyrosine kinases, including PDGFRβ, EPHA2 and EGFR, suggesting that TINCR expression might disable survival signals that are independent of BRAF or MAPK signaling. We did not investigate whether TINCR also influences the interaction between melanoma cells and the immune system. However, the TINCR transcriptional signature is enriched in genes of the immunotherapy resistance signature IPRES (Appendix Fig S5E, right panel), a signature that includes increased AXL expression and EMT gene expression and characterizes glutamine-starved melanoma cells (Hoek, 2007; Hugo *et al*, 2016; Falletta *et al*, 2017; Kozar *et al*, 2019), suggesting that TINCR also regulates the sensitivity of melanoma cells to immunotherapy with checkpoint inhibitors.

The effects of TINCR on phenotypic plasticity of melanoma cells, however, does not seem to recapitulate the typical switch between proliferative and invasive phenotypes, as initially described using melanoma cell lines (Hoek *et al*, 2008). Indeed, while TINCR modulates all the critical components of the invasive phenotype (transcriptome, protein-marker expression, *in vitro* migration, *in vivo* metastasization and drug resistance), its effect on the proliferative phenotype is far less clear. On one hand, TINCR silencing or overexpression induces, respectively, down- or up-regulation of the proliferative melanoma signature and the SOX10 proliferative marker. On the other, however, under the same experimental conditions, modulation of TINCR expression has no effects on cell proliferation, either *in vitro* or *in vivo*. Correlating the proliferative signature to proliferation has been challenging. The inverse correlation between invasion and proliferation described initially (Hoek, 2007) can be explained by the capacity of melanoma cells to maintain viability in non-permissive environments, by shifting from proliferation to quiescence and increasing motility and invasiveness (Hoek & Goding, 2010). Consistently, nutrient deprivation, as seen with glutamine starvation and hypoxia, drives invasion and restrains proliferation in melanoma cells (Falletta *et al*, 2017; Louphrasitthiphol *et al*, 2019). Induction of the invasive state, however, is consistently seen in melanoma cells also in nutrient-rich conditions, as induced by targeted therapies, signals from the TME (TNF-α; TGF-β; LIF; BMP4 or interferon) or oncogene activation (MYC expression or activation of Ha-RAS or BRAF) (Arozarena & Wellbrock, 2019). In all these cases, termed "pseudo-starvation", cells may be both invasive and proliferative. The capacity of TINCR to modulate the invasive state without affecting proliferation may reflect its involvement in signaling pathways that regulate invasion in nutrient-rich environments.

Regulation of TINCR expression, however, exerted dramatic effects on the capacity of tumors to grow locally, despite the lack of significant effects on proliferation or cell viability, suggesting additional biological effects of TINCR (Lindqvist *et al*, 2018). The "invasive phenotype" is characterized by expression signatures of melanocyte de-differentiation linked to markers of neural crest and stemness (Rambow *et al*, 2018; Larribere & Utikal, 2019). Consistently, TINCR overexpression reduced significantly the number of tumor-initiating cells, suggesting that the TINCR-induced reversion of the invasive phenotype is associated with loss of SC-like cells. Thus, reduced numbers of tumor-initiating cells may contribute to the reduced tumorigenicity of TINCR-overexpressing melanoma cells, in the absence of modifications of cell proliferation. Notably, TINCR-depleted cells showed marked increase of ATF4 expression, rate of protein synthesis and tumorigenicity. ATF4 is known to promote protein synthesis and tumorigenesis (Ye *et al*, 2010; Han *et al*, 2013), thus suggesting that ATF4 regulation by TINCR may further contribute to its effect on tumorigenicity.

We then investigated the molecular mechanisms underlying the effects of TINCR on the invasive phenotype. TINCR silencing induced marked up-regulation of the ATF4 protein and of its transcriptional program. Though ATF4 depletion had no significant effects on cell migration of melanoma proliferative phenotype cells, it rescued the increased migratory phenotype induced by TINCR depletion, suggesting that ATF4 mediates the phenotype switch induced by TINCR.

Up-regulation of the ATF4 protein during the ISR is due to increased translation of its mRNA. The ISR response is mediated by eIF2α phosphorylation, which is induced by specific kinases (PERK, PKR, GCN2 or HRI) following either starvation or pseudo-starvation signals (Garcia-Jimenez & Goding, 2019). Phosphorylated eIF2α suppresses initiation of global protein synthesis and promotes selective translation of a specific subset of ISR proteins, including ATF4 (translational reprogramming). ATF4, however, although critical, is not sufficient for the establishment of the invasive phenotype. Emerging evidence, instead, suggests that invasiveness is driven by eIF2α phosphorylation and translational reprogramming, as shown in melanoma cells following aminoacid limitation or TNF-α treatment (Falletta *et al*, 2017; Pathria *et al*, 2019), in hypoxic breast cancer cells (Sese *et al*, 2017) or during EMT in both breast and pancreatic cancer cells (Tan *et al*, 2015). TINCR silencing, instead, induces functional ATF4 and invasiveness in the absence of eIF2α phosphorylation and suppression of global protein synthesis, suggesting that TINCR regulates invasiveness through alternative signaling pathways.

Remarkably, TINCR depletion increases global protein synthesis and induces translational reprogramming. First, TINCR depletion decreased levels of phosphorylated EEF2 and increased global protein synthesis. Under starving conditions, phosphorylated EEF2 inhibits translation elongation (Proud, 2015) and stimulates the selective translation of a subset of the TOP mRNAs (Gismondi *et al*, 2014). Second, TINCR depletion induces translational reprogramming of selected transcripts, leading to increased translation of ATF4 and other ISR protein mRNAs, and decreased translation of mRNAs encoding key regulators of elongation. Thus, TINCR may regulate protein translation at multiple levels, globally, by inhibiting elongation, or specifically, increasing translational efficiency of subunits of the EIF3 translation-initiating complex (EIF3E, F, 3H and 3L) and key elongation factors (EEF2, EEF1A1, EEF1B2).

TINCR depletion also induced marked down-regulation of MITF and its target genes, suggesting that decreased MITF expression might be integral to the biological effects of TINCR depletion. Indeed, MITF is a critical regulator of phenotype switches in melanoma, as MITF-high cells are proliferative while MITF-low cells are invasive (Hoek & Goding, 2010). Ectopic expression of MITF in invasive cells, however, does not induce the proliferative switch (Carreira *et al*, 2006), suggesting that inhibition of the invasive phenotype requires other transcriptional changes. Indeed, TINCR expression keeps a hold on the expression of the invasive phenotype also in melanoma cells that do not express MITF and, most notably, reversion of the invasive phenotype by TINCR overexpression is not associated with significant effects on MITF and cell proliferation, suggesting that the capacity of TINCR to inhibit expression of the invasive phenotype is MITF-independent. As well, activation of

ATF4 following TINCR depletion is independent of MITF expression. However, whether low levels of MITF are needed to maintain the invasive phenotype induced by TINCR depletion remains unclear. Notably, overexpression of MITF reverted the stimulatory effect of shTINCR on cell migration (Appendix Figs S5F and G), suggesting that low MITF is indeed required for the inhibition of migration upon TINCR knockdown. Surprisingly, however, MITF overexpression strongly increased migration in both cell lines, and this effect was completely abrogated by the TINCR knockdown (Appendix Fig S5F and G). Since, however, the physiological significance of the effect of MITF overexpression on migration is unclear, definitive conclusions cannot be drawn from these experiments.

Finally, we investigated mechanisms of action of TINCR. lncRNAs may function through different mechanisms, depending on their cellular localization and molecules they interact with. For instance, several lncRNAs are chromatin-associated and affect transcription directly, as enhancer associated RNAs, or by transcription factor trapping, chromatin looping, or regulation of gene expression. Others may affect transcription indirectly, following their interaction with proteins (regulation of protein function, protein-protein interactions, or intracellular localization) or RNAs (regulation of mRNA stability, splicing, or translation) (Kretz et al, 2013; Sun et al, 2015). Consistently with previous reports (Kretz et al, 2013), we showed that TINCR is almost exclusively localized in the cytoplasm, where it interacts with ~ 150 unique gene-transcripts (by RNA interactome analyses). Notably, ~ 50% of the TINCR-interacting RNAs are also translationally regulated by TINCR. Among the top RNAs that are bound and translationally down-regulated by TINCR we found ATF4 and other members of ISR response. Notably, the vast majority (~ 90%) of the translationally up-regulated mRNAs were also TINCR-interacting, suggesting that one critical function of TINCR is to bind specific mRNAs and reduce their binding to the 80S translating ribosomes (translational reprogramming). This represents a novel function of TINCR. In the epidermis, TINCR mediates the stabilization of key keratinocyte-differentiation genes through direct binding to staufen (STAU1) and target mRNAs (Kretz et al, 2013; Sun et al, 2015). In melanoma cells, however, only a marginal fraction (~ 10%) of the TINCR-interacting mRNAs showed altered stability.

In conclusion, we showed that the TINCR lncRNA interacts with RNAs associated with the invasive phenotype, preventing their binding to the translating ribosomes, and that its expression in melanoma functions as a barrier for the acquisition of the invasive phenotype, including drug resistance and dissemination. Notably, the effect of TINCR depends on ATF4 expression, but is independent of known pathways associated with the regulation of the ISR and plasticity in melanoma, including MITF, eIF2α, and TOR, and appears to function in nutrient-rich conditions. Further characterization of the upstream signaling pathways that regulate TINCR expression may provide novel targets for the suppression of the invasive phenotype in melanoma.

Materials and Methods

Plasmids

MISSION lentiviral pLKO.1 constructs containing TINCR shRNAs or scrambled non-targeting shRNAs (Sigma-Aldrich, Cat # SHCLND-NM_153375;

shRNA sequences: shTINCR-1 CCGGCTGCTGTGTGACTTTGAGGTTCT CGAGAACCTCAAAGTCACACAGCAGTTTTTTG; shTINCR- 2: CCGGGTT CTGAAGAACTCTGGCCAACTCGAGTTGGCCAGAGTTCTTCAGAACTT TTTTG) were used to knockdown TINCR RNA. TINCR full-length cDNA (3.73 Kb, transcript ID ENST00000448587.5 (Ensembl) was cloned using pCR™8/GW/TOPO™ TA Cloning Kit (Thermo Fisher Scientific, Cat # K250020). The recombinant entry clones plasmids were sequence verified and transduced into pLenti PGK PURO DEST destination vector (Addgene, Cat # 59151) using Gateway™ LR Clonase™ Enzyme mix (Thermo Fisher Scientific, Cat # 11791-020).

Lentiviral transduction

The HEK-293T packaging cells were transfected using the calcium phosphate method with lentiviral expression vectors as previously described (Bossi et al, 2016). Infections were performed for 16 h in standard medium supplemented with 4 µg/ml polybrene. The viral-containing supernatants were collected at 48 h and used to infected melanoma cells. 48 h post-infection, the medium was replaced and puromycin (2 µg/ml) added for additional 3 days.

RNA preparation and quantitative PCR analysis

Total RNA was extracted from cells using QIAzol reagent (QIAGEN, Cat # 79306), treated with TURBO DNAse1 (Thermo Fischer Scientific, Cat # AM2238). 1 µg of RNA was oligo dT primed and reverse transcribed using Reverse Transcription Kit (Promega, Cat # A3800), according to manufacturer's indications. The cDNA samples were diluted to 20 ng/µl. All real-time PCR reactions were performed using the ABI 7700 sequence detection system (Perkin Elmer Applied Biosystems), and the amplifications were done using the SYBR Green PCR Master Mix (Thermo Fisher Scientific, Cat # 4385612). The thermal cycling conditions were composed of 50°C for 2 min followed by an initial denaturation step at 95°C for 10 min, 40 cycles at 95°C for 30 s, 60°C for 30 s, and 72°C for 30 s. The experiments were carried out in duplicate for each data point. The relative quantification in gene expression was determined using the $2^{-\Delta Ct}$ method. The housekeeping gene L32P was used as normalizer. The following qPCR primers were used: TINCR_forward: TGTGGCCCAAACTCAGGGATACAT, TINCR_reverse: AGATGACAGTGGCTGGAGTTGTCA; L32P_forward: AGGCATTGACAACAGGGTTC; L32P_reverse: GTTGCACATCAGCAG-CACTT; ATF4_forward: ATGACCGAAATGAGCTTCCTG, ATF4_reverse: GCTGGAGAACCCATGAGGT.

RNA sequencing (RNA-seq)

Total RNA from melanoma cell cultures, or from nevi, primary and metastatic melanoma clinical specimens was extracted using QIAzol reagent (QIAGEN) and the quality assessed on the 2100 Bioanalyzer (Agilent). RNA-seq libraries were prepared from 1µg of total RNA using the TruSeq RNA Library Preparation Kit v2 (Illumina, Cat # RS-122-2001) according to manufacturer instructions. The libraries were sequenced on an HiSeq™ 2000 Sequencing System (Illumina).

RNA-seq analysis

50 bp paired-end RNA-seq reads were aligned to genome (hg19, GRCh38) using TopHat2 2.0.9 (Kim et al, 2013) starting from

3×10^7 mapped paired-end reads per sample. Read counts of each gene were quantified using HTseq (Anders *et al*, 2015) and differential analysis was performed using DESeq or edgeR bioconductor packages. Gene set enrichment analysis was also performed using GSEA (Gene Set Enrichment Analysis) software v2.2.0 (Subramanian *et al*, 2005) with GO biological process and MSigDB gene sets using default parameters. Gene sets enriched at FDR < 0.25 were considered statistically significant.

Western blot analysis

Total protein extracts were prepared by directly lysing the cells in RIPA buffer (10 mM Tris (pH 8.0), 150 mM NaCl, 1% Triton-X100, 0.5% sodium deoxycholate, 0.1% sodium dodecyl sulfate, SDS), containing 5% glycerol, 1.5 mM MgCl$_2$, Pierce™ protease and phosphatase inhibitors (Thermo Fisher Scientific, Cat # A32957 and A32963). Lysates were incubated on ice for 20 min, sonicated three times for 10 s and centrifuged at 20,000 *g* for 30 min. Protein concentration was determined using the protein assay reagent (BioRad). Proteins were separated by SDS–PAGE, transferred to a PVDF membrane (Millipore), and detected using the following antibodies against: anti-4EBP1 (Cell Signaling Technology, Cat # 9644); anti-ATF4 (Cell Signaling Technology, Cat # 11815); anti-AXL (Santa Cruz Biotechnology, Cat # sc-166269); anti-CHOP (Cell Signaling Technology, Cat # 2895); anti-cleaved Caspase 3 (Abcam, Cat # ab2302); Anti-EGFR (Cell Signaling Technology, Cat # 4267); anti-eIF2α (Santa Cruz Biotechnology, Cat # sc-133132); anti-EPHA2 (Cell Signaling, Cat # 6997); anti-Ki67, (Thermo Fisher Scientific, Cat # MA5-14520); anti-MITF (Abcam, Cat # ab12039); anti-N-cadherin (BD biosciences, Cat # 610921); anti-PDGFRβ (Cell Signaling Technology, Cat # 3169); anti-phospho 4EBP1 (Cell Signaling Technology, Cat # 2855S); anti-phospho S51 eIF2a (Cell Signaling Technology, Cat # 9721); anti-phospho S6 kinase (Cell Signaling Technology, Cat # 9204); anti-S6 kinase (Cell Signaling Technology, Cat # 2708); anti-SNAI1 (Cell Signaling Technology, Cat # 3879); anti-SOX10 (Cell Signaling Technology, Cat # 89356); anti-ZEB1 (Thermo Fischer Scientific, Cat # PA5-28221); anti-GAPDH, (Sigma-Aldrich, Cat # G8795); Anti-Vinculin (Sigma-Aldrich, Cat # 9131); anti-Tubulin (Sigma-Aldrich, Cat # T9026). GAPDH, Tubulin and Vinculin were used as loading controls.

Cell proliferation, cell migration, spheroid invasion assay and drug-response assays

All experiments were performed 96 h after lentiviral transduction. For cell proliferation assays, cells were seeded in 96-well plates (5,000 cells/well) and cell viability was assessed for 5 days with *CellTiter-Glo* Luminescent Cell Viability Assay (Promega, Cat # G7570), according to manufacturer's instructions. For cell migration assays, 50,000 cells were seeded in duplicates on fibronectin precoated, transwell permeable supports (6.5 mm, 8.0 μm pore size, Corning, Cat # CLS3464) in medium without serum. Medium containing 10% FBS was used as chemoattractant. Migrated cells were visualized after 8–16 h by crystal violet staining and quantified by ImageJ (NIH). Two-tailed Student's *t*-test was used to analyze data from three independent experiments.

For collagen invasion assay, MM13 and WM902B cells (1,000/2,000/4,000) were seeded as hanging drops in their complete culture medium +0.2% methylcellulose for 72 h.

Spheroids were then embedded in 1 mg/ml collagen matrix (Collagen I rat tail Corning # 354249, diluted in serum-free medium) in 96-well plates. Spheroids were monitored over time and pictures were taken at EVOS microscope. Spheroid spreading area was measured with ImageJ, by manually identifying the spheroid invasion front. Invasion rate was then calculated as ratio between the area at 24 and zero time points after plating.

For dose-response curves, cells were plated in 96-well plates (5,000 cells/well) 24 h prior drug treatment and incubated for 72 h with PLX4032 (Vemurafenib, Cat # A-1130) and GSK1120212 (Trametinib, Cat # A-1258) purchased from Active Biochemicals (Kowloon, Hong Kong). Cell viability was assessed with the *CellTiter-Glo* Luminescent Cell Viability Assay. The dose-response curve was fit with the nonlinear regression using GraphPad Prism software.

In vivo studies

Infected melanoma cells were intradermally injected in quadruplicate into NOD.Cg-Prkdcscid Il2rgtm1Wjl/SzJ (NSG) mice. We used 400,000, 600,000, and 200,000 cells/mouse for WM1552C, WM902B and MM13 PDX cells, respectively, resuspended in a 3:1 mix of L15 medium and Matrigel Matrix HC (Corning, Cat # 354248). The experiments were performed in duplicate, using four mice per group (shSCR/sh*TINCR* or Empty vector/*TINCR*) per experiment. Metastasis formation was evaluated in MM13 transplanted mice, 4 weeks after the resection of primary tumors. Mice were sacrificed and metastases at lymph nodes, lungs and liver collected.

Extreme limiting dilution assay (ELDA)

MM13 PDX cells were infected *in vitro* with PGK puro lentiviral vector overexpressing *TINCR* or with Empty vector. After 3 days of selection with Puromycin, 10,000, 1,000, 100, 10, or 1 cells per group were subcutaneously injected in immunocompromised mice as previously reported by Bossi *et al* (2016). Mice were monitored weekly for tumor formation or any sign of illness/weakness, and they were sacrificed when tumors reached a maximum volume of 0.6–0.8 cm^3. The frequency of CSCs was calculated as reported previously (Hu & Smyth, 2009) using publicly available website http://bioinf.wehi.edu.au/software/elda/. Differences among groups were considered significant for $P < 0.05$.

Immunohistochemistry

Tissues were surgically removed, fixed with 4% (wt/vol) paraformaldehyde, paraffin-embedded, and sectioned. Sections were deparaffinized by xylene and re-hydrated in graded alcohol. Slides were preincubated with blocking solution (Kretz *et al*, 2013), 2% (wt/vol) BSA, 2% (vol/vol) normal goat serum, and 0.02% Tween 20 in Tris-buffered saline (pH 7.4) and then stained with primary antibodies overnight at 4°C. Slides were incubated with secondary antibody (HRP rabbit or mouse antibody; DAKO EnVision System, Agilent, Cat # K4065) for 30 min at room temperature. After washing, sections were incubated in peroxidase substrate solution (DAB; DAKO, Agilent, Cat # GV825), rinsed in water, and counterstained with hematoxylin. Immunohistochemistry was performed with anti-Ki-67 (Cat #14-5698-82), anti-cleaved Caspase 3 (Abcam, Cat # ab2302) antibodies. Images were acquired with OLYMPUS BX51 up-

right microscope (UPIanAPO 40×/0.85 objective lenses) connected to Nikon color Camera Digital Sight DS-U1 and analyzed with the NIS-elements software. Randomly taken images (at least five fields per animal) were captured from tissue sections and processed with ImageJ software (National Institutes of Health).

RNA interactome sequencing (RIA-seq)

TINCR RNA interactome analysis was performed using antisense DNA 3′-biotin-TEG oligonucleotide probes described in (Kretz *et al*, 2013). RNA interactome pulldown was carried out according to previously published protocol (Damas *et al*, 2016). In brief, 3×10^7 cells were crosslinked with 1% glutaraldehyde for 10 min at room temperature and lysed in 2 ml of lysis buffer (50 mM Tris, pH 7.0, 10 mM EDTA, 1% SDS, dithiothreitol (DTT), phenyl-methylsulfonyl fluoride (PMSF), Pierce™ protease inhibitor cocktail (Thermo Fisher Scientific, Cat #32963) and SUPERase-In™ RNase inhibitor (Thermo Fischer Scientific, Cat # AM2694) on ice for 10 min. The lysates were sonicated using Bioruptor (Diagenode) for 20 cycles (30″ ON; 30″ OFF). Cell lysate was diluted in double the volume of hybridization buffer (500 mM NaCl, 1% SDS, 100 mM Tris, pH 7.0, 10 mM EDTA, 15% formamide), and added just before use: 1 mM DTT, 1 mM PMSF, protease inhibitor, and SUPERase-In™ RNase inhibitor. 100 pmol probes were added to 3 ml of diluted lysate and incubated at end-to-end rotation at 37°C for 4 h. Streptavidin-magnetic C1 beads (Thermo Fischer Scientific, Cat # 65001) were washed three times in cell lysis buffer, 100 μl of beads were added to hybridization mix and incubated for 30 min. The samples were washed three times by washing buffer (2×SSC, 0.5% SDS, 1 mM PMSF, SUPERase-In™ RNase inhibitor). RNA was eluted from beads in 200 μl RNA proteinase K buffer (100 mM NaCl, 10 mM Tris, pH 7.0, 1 mM EDTA, 0.5% SDS) and 1 mg/ml proteinase K (Thermo Fisher Scientific, Cat # 25530049) at 50°C for 45 min and purified by QIAzol (QIAGEN) reagent. 80 ng of RNA from each sample was used for library preparation using Illumina Truseq V2 kit (Cat # RS-122-2001).

In vivo [35S] metabolic labeling

The cells were starved for 30 min in Methionine-Cysteine-free DMEM (Thermo Fisher Cat # 21013024) and pulse labeled with 0.7 mCi/ml of 35S-Methionine-Cysteine mix (EASYTAG™ Protein Labeling Mix, Perkin Elmer Cat # NEG709A001MC) for 5 min. Cells were lysed immediately in RIPA buffer and subjected to SDS–PAGE analysis. Autoradiography images were acquired using Typhoon Biomolecular Imager (Amersham). For quantification of [35S]-amino acid incorporation 50 microliters of cell extracts were precipitated with 10% trichloracetic acid (TCA) transferred on 3MM filters and subjected to liquid scintillation counting (Packard 2000TR, Perkin Elmer).

RIA-seq data analysis

The reads were trimmed from trailing adapter sequences using Fastx tool kit and aligned to genome (hg19, GRCh38) using TopHat2 2.0.9 (Kim *et al*, 2013). Peak calling was performed using exomePeak Bioconductor package (Meng *et al*, 2013) using default parameters. Peaks present in both odd and even pulldowns were used for further

analysis. Gene set enrichment analysis was carried out as described above.

Ribosome profiling

Libraries of ribosome-protected fragments (RPFs) were generated using the mammalian TruSeq Ribo Profile Library Prep Kit (Illumina, Cat # RPYSC12116). The experiment was done in two biological replicates for each condition. Briefly, cell cultures were treated with cycloheximide at 0.1 mg/ml for 5 min and lysed according to the manufacturer's instructions. To generate Ribosome Footprints, cell lysates were digested with TruSeq Ribo Profile Nuclease. The ribosome-protected fragments were first purified using MicroSpin S-400 columns (GE Lifesciences, Cat # 27514001) and then size-selected (28–30 nt) from 15% polyacrylamide/7–8 M urea/TBE gel. rRNA was removed using the Ribo-Zero rRNA Removal Kit (Illumina, Cat # RZH1046). After 30′ adaptor ligation and reverse transcription of the library, cDNA (70-80 nt) was purified from 10% polyacrylamide/7–8 M urea/TBE gel. After cDNA circularization and limited amplification (nine cycles), the RPF libraries were purified using an 8% native polyacrylamide gel. The RPF and mRNA libraries were sequenced on an Illumina HiSeq 2500 sequencer with single-end 50 cycles (SE50) run type.

Ribosome profiling data analysis

Sequencing reads were clipped for 3′ adapter sequences quality filtered (Phred quality score 33) and the reads longer than 25 bp were kept for further analysis. The reads were aligned to genome (hg19, GRCh38) using TopHat2 2.0.9 (Kim *et al*, 2013). Quality control of RPF libraries and ORF identification were carried out with Ribotaper package (Calviello *et al*, 2016). Differential translation analysis was performed using Xtail Bioconductor package (Xiao *et al*, 2016). Gene set enrichment analysis was carried out as described above.

Analysis of the TCGA SKCM dataset

Quantile normalized level_3 RNA-seqV2 TCGA dataset (445 samples of skin cutaneous melanoma, SKCM) was downloaded from Firehose (Broad Institute). Sample clustering was performed using the ConsensusClusterPlus R/Bioconductor package (Wilkerson & Hayes, 2010). The analysis of differential expression between the two groups of primary melanomas was performed using DSESq R/Bioconductor package (Anders & Huber, 2010). The primary melanoma gene signature was defined by those genes showing a 1.5-fold difference and an adjusted P value < 0.05. This list was used to conduct Qiagen IPA (Ingenuity Systems) and GSEA enrichment analysis (Subramanian *et al*, 2005) using GO terms and MSigDB datasets. Somatic mutation calls for 345 SKCM samples were downloaded from Firehose. The association between BRAF and NRAS hotspot mutations with cluster assignment was evaluated using the χ^2 test. Illumina Infinium Human DNA Methylation 450 level 3 DNA methylation Data for SKCM TCGA dataset containing mean beta values for each gene were downloaded from the Broad GDAC Firehose. The correlation between differential methylation and differential expression of each gene in the primary melanoma gene signature was calculated using the Spearman

correlation coefficient. False discovery rate (FDR) was calculated using Benjamini–Hochberg correction. *TINCR* gene DNA copy number calls from SKCM TCGA dataset were downloaded from the Cbioportal.org. The association between copy number variation and gene expression clusters was calculated using the Kruskal–Wallis test. Copy number variation analysis of *TINCR* gene on SKCM TCGA dataset was performed by the Cbioportal tool (www.cbioportal.org) using the GISTIC algorithm. Copy number status of the gene was defined as follows: "−2" is a deep loss, possibly a homozygous deletion, "−1" is a shallow loss (possibly heterozygous deletion), "0" is diploid, "1" indicates a low-level gain, and "2" is a high-level amplification.

Statistics

Experimental data were analyzed with GraphPad Prism 5 and were presented as mean ± s.e.m. or mean ± s.d. as indicated. Two-tailed Student's t-test was used to compare means between groups as indicated, and $P < 0.05$ was considered significant. For Western blot results, representative figures from three or more independent experiments were shown.

Associations between categorical variables were evaluated using the Pearson's χ^2 test or Fisher's exact test, as appropriate. Non-parametric correlations were tested by the Spearman's rank coefficient. Continuous variables with a non-normal distribution were compared between two groups using the Mann–Whitney U-test, and between more than two groups using Kruskal–Wallis H-test.

Data availability

The access number for the RIA-seq, RNA-seq and Ribo-seq deposited data reported in this study is NCBI GEO: GSE125835 (http://www.ncbi.nlm.nih.gov/geo/query/acc.cgi?acc=GSE125835). Data analysis was performed using publicly available software, listed in the Materials and Methods section.

Expanded View for this article is available online.

Author contributions

Conception and Design: MMe, DB, SM, LL, PGP. Development of methodology: MMe, DB, GT. Acquisition of data (provided animals and facilities, managed experimental assays): MMe, DB, SP, FM, MMi, AC. Analysis and interpretation of data: MMe, DB, TB, JC-M, EL, IB. Writing, review and/or revision of manuscript: MMe, JC-M, EL, PGP, LL. Study supervision: LL, PGP.

Conflict of interest

The authors declare that they have no conflict of interest.

References

Anders S, Huber W (2010) Differential expression analysis for sequence count data. *Genome Biol* 11: R106

Anders S, Pyl PT, Huber W (2015) HTSeq–a Python framework to work with high-throughput sequencing data. *Bioinformatics* 31: 166−169

Arozarena I, Wellbrock C (2019) Phenotype plasticity as enabler of melanoma progression and therapy resistance. *Nat Rev Cancer* 19: 377−391

Bhan A, Soleimani M, Mandal SS (2017) Long noncoding RNA and cancer: a new paradigm. *Cancer Res* 77: 3965−3981

Bondurand N, Pingault V, Goerich DE, Lemort N, Sock E, Le Caignec C, Wegner M, Goossens M (2000) Interaction among SOX10, PAX3 and MITF, three genes altered in Waardenburg syndrome. *Hum Mol Genet* 9: 1907−1917

Boshuizen J, Koopman LA, Krijgsman O, Shahrabi A, van den Heuvel EG, Ligtenberg MA, Vredevoogd DW, Kemper K, Kuilman T, Song JY *et al* (2018) Cooperative targeting of melanoma heterogeneity with an AXL antibody-drug conjugate and BRAF/MEK inhibitors. *Nat Med* 24: 203−212

Bossi D, Cicalese A, Dellino GI, Luzi L, Riva L, D'Alesio C, Diaferia GR, Carugo A, Cavallaro E, Piccioni R *et al* (2016) *In vivo* genetic screens of patient-derived tumors revealed unexpected frailty of the transformed phenotype. *Cancer Discov* 6: 650−663

Calviello L, Mukherjee N, Wyler E, Zauber H, Hirsekorn A, Selbach M, Landthaler M, Obermayer B, Ohler U (2016) Detecting actively translated open reading frames in ribosome profiling data. *Nat Methods* 13: 165−170

Carreira S, Goodall J, Denat L, Rodriguez M, Nuciforo P, Hoek KS, Testori A, Larue L, Goding CR (2006) Mitf regulation of Dia1 controls melanoma proliferation and invasiveness. *Genes Dev* 20: 3426−3439

Cheli Y, Giuliano S, Botton T, Rocchi S, Hofman V, Hofman P, Bahadoran P, Bertolotto C, Ballotti R (2011) Mitf is the key molecular switch between mouse or human melanoma initiating cells and their differentiated progeny. *Oncogene* 30: 2307−2318

Chen X, Sun Y, Cai R, Wang G, Shu X, Pang W (2018) Long noncoding RNA: multiple players in gene expression. *BMB Rep* 51: 280−289

Coe EA, Tan JY, Shapiro M, Louphrasitthiphol P, Bassett AR, Marques AC, Goding CR, Vance KW (2019) The MITF-SOX10 regulated long non-coding RNA DIRC3 is a melanoma tumour suppressor. *PLoS Genet* 15: e1008501

Damas ND, Marcatti M, Come C, Christensen LL, Nielsen MM, Baumgartner R, Gylling HM, Maglieri G, Rundsten CF, Seemann SE *et al* (2016) SNHG5 promotes colorectal cancer cell survival by counteracting STAU1-mediated mRNA destabilization. *Nat Commun* 7: 13875

Damsky WE, Theodosakis N, Bosenberg M (2014) Melanoma metastasis: new concepts and evolving paradigms. *Oncogene* 33: 2413−2422

Ennen M, Keime C, Kobi D, Mengus G, Lipsker D, Thibault-Carpentier C, Davidson I (2015) Single-cell gene expression signatures reveal melanoma cell heterogeneity. *Oncogene* 34: 3251−3263

Falletta P, Sanchez-Del-Campo L, Chauhan J, Effern M, Kenyon A, Kershaw CJ, Siddaway R, Lisle R, Freter R, Daniels MJ *et al* (2017) Translation reprogramming is an evolutionarily conserved driver of phenotypic plasticity and therapeutic resistance in melanoma. *Genes Dev* 31: 18−33

Ferguson J, Smith M, Zudaire I, Wellbrock C, Arozarena I (2017) Glucose availability controls ATF4-mediated MITF suppression to drive melanoma cell growth. *Oncotarget* 8: 32946−32959

Gao M, Liu Y, Chen Y, Yin C, Chen JJ, Liu S (2016) miR-214 protects erythroid cells against oxidative stress by targeting ATF4 and EZH2. *Free Radic Biol Med* 92: 39 – 49

Garcia-Jimenez C, Goding CR (2019) Starvation and pseudo-starvation as drivers of cancer metastasis through translation reprogramming. *Cell Metab* 29: 254 – 267

Gismondi A, Caldarola S, Lisi G, Juli G, Chellini L, Iadevaia V, Proud CG, Loreni F (2014) Ribosomal stress activates eEF2K-eEF2 pathway causing translation elongation inhibition and recruitment of terminal oligopyrimidine (TOP) mRNAs on polysomes. *Nucleic Acids Res* 42: 12668 – 12680

Goding CR, Arnheiter H (2019) MITF-the first 25 years. *Genes Dev* 33: 983 – 1007

Goodall J, Carreira S, Denat L, Kobi D, Davidson I, Nuciforo P, Sturm RA, Larue L, Goding CR (2008) Brn-2 represses microphthalmia-associated transcription factor expression and marks a distinct subpopulation of microphthalmia-associated transcription factor-negative melanoma cells. *Cancer Res* 68: 7788 – 7794

Gugnoni M, Ciarrocchi A (2019) Long noncoding RNA and epithelial mesenchymal transition in cancer. *Int J Mol Sci* 20: 1924

Han J, Back SH, Hur J, Lin YH, Gildersleeve R, Shan J, Yuan CL, Krokowski D, Wang S, Hatzoglou M *et al* (2013) ER-stress-induced transcriptional regulation increases protein synthesis leading to cell death. *Nat Cell Biol* 15: 481 – 490

He L, Yuan J, Xu Q, Chen R, Chen L, Fang M (2016) miRNA-1283 regulates the PERK/ATF4 pathway in vascular injury by targeting ATF4. *PLoS One* 11: e0159171

Hoek KS (2007) DNA microarray analyses of melanoma gene expression: a decade in the mines. *Pigment Cell Res* 20: 466 – 484

Hoek KS, Eichhoff OM, Schlegel NC, Dobbeling U, Kobert N, Schaerer L, Hemmi S, Dummer R (2008) *In vivo* switching of human melanoma cells between proliferative and invasive states. *Can Res* 68: 650 – 656

Hoek KS, Goding CR (2010) Cancer stem cells versus phenotype-switching in melanoma. *Pigment Cell Melanoma Res* 23: 746 – 759

Hu Y, Smyth GK (2009) ELDA: extreme limiting dilution analysis for comparing depleted and enriched populations in stem cell and other assays. *J Immunol Methods* 347: 70 – 78

Huarte M (2015) The emerging role of lncRNAs in cancer. *Nat Med* 21: 1253 – 1261

Hugo W, Zaretsky JM, Sun L, Song C, Moreno BH, Hu-Lieskovan S, Berent-Maoz B, Pang J, Chmielowski B, Cherry G *et al* (2016) Genomic and transcriptomic features of response to anti-PD-1 therapy in metastatic melanoma. *Cell* 165: 35 – 44

Ingolia NT, Hussmann JA, Weissman JS (2019) Ribosome profiling: global views of translation. *Cold Spring Harb Perspect Biol* 11: a032698

Jaberg-Bentele NF, Kunz M, Abuhammad S, Dummer R (2017) Flare-up of rheumatoid arthritis by anti-CTLA-4 antibody but not by anti-PD1 therapy in a patient with metastatic melanoma. *Case Rep Dermatol* 9: 65 – 68

Jenkins RW, Barbie DA, Flaherty KT (2018) Mechanisms of resistance to immune checkpoint inhibitors. *Br J Cancer* 118: 9 – 16

Johansson JA, Marie KL, Lu Y, Brombin A, Santoriello C, Zeng Z, Zich J, Gautier P, von Kriegsheim A, Brunsdon H *et al* (2020) PRL3-DDX21 transcriptional control of endolysosomal genes restricts melanocyte stem cell differentiation. *Dev Cell* 54: 317 – 332

Kedersha N, Chen S, Gilks N, Li W, Miller IJ, Stahl J, Anderson P (2002) Evidence that ternary complex (eIF2-GTP-tRNA(i)(Met))-deficient preinitiation complexes are core constituents of mammalian stress granules. *Mol Biol Cell* 13: 195 – 210

Kim D, Pertea G, Trapnell C, Pimentel H, Kelley R, Salzberg SL (2013) TopHat2: accurate alignment of transcriptomes in the presence of insertions, deletions and gene fusions. *Genome Biol* 14: R36

Kim IS, Heilmann S, Kansler ER, Zhang Y, Zimmer M, Ratnakumar K, Bowman RL, Simon-Vermot T, Fennell M, Garippa R *et al* (2017) Microenvironment-derived factors driving metastatic plasticity in melanoma. *Nat Commun* 8: 14343

Knight JRP, Garland G, Poyry T, Mead E, Vlahov N, Sfakianos A, Grosso S, De-Lima-Hedayioglu F, Mallucci GR, von der Haar T *et al* (2020) Control of translation elongation in health and disease. *Dis Models Mech* 13: dmm043208

Konieczkowski DJ, Johannessen CM, Abudayyeh O, Kim JW, Cooper ZA, Piris A, Frederick DT, Barzily-Rokni M, Straussman R, Haq R *et al* (2014) A melanoma cell state distinction influences sensitivity to MAPK pathway inhibitors. *Cancer Discov* 4: 816 – 827

Kozar I, Margue C, Rothengatter S, Haan C, Kreis S (2019) Many ways to resistance: how melanoma cells evade targeted therapies. *Biochim Biophys Acta Rev Cancer* 1871: 313 – 322

Kretz M, Siprashvili Z, Chu C, Webster DE, Zehnder A, Qu K, Lee CS, Flockhart RJ, Groff AF, Chow J *et al* (2013) Control of somatic tissue differentiation by the long non-coding RNA TINCR. *Nature* 493: 231 – 235

Kunz M, Holzel M (2017) The impact of melanoma genetics on treatment response and resistance in clinical and experimental studies. *Cancer Metastasis Rev* 36: 53 – 75

Landsberg J, Kohlmeyer J, Renn M, Bald T, Rogava M, Cron M, Fatho M, Lennerz V, Wolfel T, Holzel M *et al* (2012) Melanomas resist T-cell therapy through inflammation-induced reversible dedifferentiation. *Nature* 490: 412 – 416

Larribere L, Utikal J (2019) Stem cell-derived models of neural crest are essential to understand melanoma progression and therapy resistance. *Front Mol Neurosci* 12: 111

Laurette P, Strub T, Koludrovic D, Keime C, Le Gras S, Seberg H, Van Otterloo E, Imrichova H, Siddaway R, Aerts S *et al* (2015) Transcription factor MITF and remodeller BRG1 define chromatin organisation at regulatory elements in melanoma cells. *Elife* 4: e06857

Lee M, Goodall J, Verastegui C, Ballotti R, Goding CR (2000) Direct regulation of the Microphthalmia promoter by Sox10 links Waardenburg-Shah syndrome (WS4)-associated hypopigmentation and deafness to WS2. *J Biol Chem* 275: 37978 – 37983

Lessard L, Liu M, Marzese DM, Wang H, Chong K, Kawas N, Donovan NC, Kiyohara E, Hsu S, Nelson N *et al* (2015) The CASC15 long intergenic noncoding RNA locus is involved in melanoma progression and phenotype switching. *J Invest Dermatol* 135: 2464 – 2474

Leucci E, Coe EA, Marine JC, Vance KW (2016a) The emerging role of long non-coding RNAs in cutaneous melanoma. *Pigment Cell Melanoma Res* 29: 619 – 626

Leucci E, Vendramin R, Spinazzi M, Laurette P, Fiers M, Wouters J, Radaelli E, Eyckerman S, Leonelli C, Vanderheyden K *et al* (2016b) Melanoma addiction to the long non-coding RNA SAMMSON. *Nature* 531: 518 – 522

Lindqvist LM, Tandoc K, Topisirovic I, Furic L (2018) Cross-talk between protein synthesis, energy metabolism and autophagy in cancer. *Curr Opin Genet Dev* 48: 104 – 111

Louphrasitthiphol P, Ledaki I, Chauhan J, Falletta P, Siddaway R, Buffa FM, Mole DR, Soga T, Goding CR (2019) MITF controls the TCA cycle to modulate the melanoma hypoxia response. *Pigment Cell Melanoma Res* 32: 792 – 808

Louphrasitthiphol P, Siddaway R, Loffreda A, Pogenberg V, Friedrichsen H, Schepsky A, Zeng Z, Lu M, Strub T, Freter R *et al* (2020) Tuning

transcription factor availability through acetylation-mediated genomic redistribution. *Mol Cell* 79: 472–487

McMahon M, Samali A, Chevet E (2017) Regulation of the unfolded protein response by noncoding RNA. *Am J Physiol Cell Physiol* 313: C243–C254

Meng J, Cui X, Rao MK, Chen Y, Huang Y (2013) Exome-based analysis for RNA epigenome sequencing data. *Bioinformatics* 29: 1565–1567

Meyuhas O, Kahan T (2015) The race to decipher the top secrets of TOP mRNAs. *Biochim Biophys Acta* 1849: 801–811

Muller J, Krijgsman O, Tsoi J, Robert L, Hugo W, Song C, Kong X, Possik PA, Cornelissen-Steijger PD, Geukes Foppen MH *et al* (2014) Low MITF/AXL ratio predicts early resistance to multiple targeted drugs in melanoma. *Nat Commun* 5: 5712

Nandagopal N, Roux PP (2015) Regulation of global and specific mRNA translation by the mTOR signaling pathway. *Translation (Austin)* 3: e983402

O'Connell MP, Marchbank K, Webster MR, Valiga AA, Kaur A, Vultur A, Li L, Herlyn M, Villanueva J, Liu Q *et al* (2013) Hypoxia induces phenotypic plasticity and therapy resistance in melanoma via the tyrosine kinase receptors ROR1 and ROR2. *Cancer Discov* 3: 1378–1393

Pakos-Zebrucka K, Koryga I, Mnich K, Ljujic M, Samali A, Gorman AM (2016) The integrated stress response. *EMBO Rep* 17: 1374–1395

Pathria G, Lee JS, Hasnis E, Tandoc K, Scott DA, Verma S, Feng Y, Larue L, Sahu AD, Topisirovic I *et al* (2019) Translational reprogramming marks adaptation to asparagine restriction in cancer. *Nat Cell Biol* 21: 1590–1603

Pavitt GD (2018) Regulation of translation initiation factor eIF2B at the hub of the integrated stress response. *Wiley Interdiscip Rev RNA* 9: e1491

Phung B, Ciesla M, Sanna A, Guzzi N, Beneventi G, Cao Thi Ngoc P, Lauss M, Cabrita R, Cordero E, Bosch A *et al* (2019) The X-Linked DDX3X RNA helicase dictates translation reprogramming and metastasis in melanoma. *Cell Rep* 27: 3573–3586

Pichon X, Wilson LA, Stoneley M, Bastide A, King HA, Somers J, Willis AE (2012) RNA binding protein/RNA element interactions and the control of translation. *Curr Protein Pept Sci* 13: 294–304

Pinner S, Jordan P, Sharrock K, Bazley L, Collinson L, Marais R, Bonvin E, Goding C, Sahai E (2009) Intravital imaging reveals transient changes in pigment production and Brn2 expression during metastatic melanoma dissemination. *Cancer Res* 69: 7969–7977

Potterf SB, Furumura M, Dunn KJ, Arnheiter H, Pavan WJ (2000) Transcription factor hierarchy in Waardenburg syndrome: regulation of MITF expression by SOX10 and PAX3. *Hum Genet* 107: 1–6

Proud CG (2015) Regulation and roles of elongation factor 2 kinase. *Biochem Soc Trans* 43: 328–332

Qin X, Jiang B, Zhang Y (2016) 4E-BP1, a multifactor regulated multifunctional protein. *Cell Cycle* 15: 781–786

Rambow F, Rogiers A, Marin-Bejar O, Aibar S, Femel J, Dewaele M, Karras P, Brown D, Chang YH, Debiec-Rychter M *et al* (2018) Toward minimal residual disease-directed therapy in melanoma. *Cell* 174: 843–855

Rambow F, Marine JC, Goding CR (2019) Melanoma plasticity and phenotypic diversity: therapeutic barriers and opportunities. *Genes Dev* 33: 1295–1318

Riesenberg S, Groetchen A, Siddaway R, Bald T, Reinhardt J, Smorra D, Kohlmeyer J, Renn M, Phung B, Aymans P *et al* (2015) MITF and c-Jun antagonism interconnects melanoma dedifferentiation with pro-inflammatory cytokine responsiveness and myeloid cell recruitment. *Nat Commun* 6: 8755

Saxton RA, Sabatini DM (2017) mTOR signaling in growth, metabolism, and disease. *Cell* 169: 361–371

Schadendorf D, van Akkooi ACJ, Berking C, Griewank KG, Gutzmer R, Hauschild A, Stang A, Roesch A, Ugurel S (2018) Melanoma. *Lancet* 392: 971–984

Sensi M, Catani M, Castellano G, Nicolini G, Alciato F, Tragni G, De Santis G, Bersani I, Avanzi G, Tomassetti A *et al* (2011) Human cutaneous melanomas lacking MITF and melanocyte differentiation antigens express a functional Axl receptor kinase. *J Invest Dermatol* 131: 2448–2457

Sese M, Fuentes P, Esteve-Codina A, Bejar E, McGrail K, Thomas G, Aasen T, Ramon YCS (2017) Hypoxia-mediated translational activation of ITGB3 in breast cancer cells enhances TGF-beta signaling and malignant features *in vitro* and *in vivo*. *Oncotarget* 8: 114856–114876

Staaf J, Harbst K, Lauss M, Ringner M, Masback A, Howlin J, Jirstrom K, Harland M, Zebary A, Palmer JM *et al* (2014) Primary melanoma tumors from CDKN2A mutation carriers do not belong to a distinct molecular subclass. *J Invest Dermatol* 134: 3000–3003

Subramanian A, Tamayo P, Mootha VK, Mukherjee S, Ebert BL, Gillette MA, Paulovich A, Pomeroy SL, Golub TR, Lander ES *et al* (2005) Gene set enrichment analysis: a knowledge-based approach for interpreting genome-wide expression profiles. *Proc Natl Acad Sci USA* 102: 15545–15550

Sun BK, Boxer LD, Ransohoff JD, Siprashvili Z, Qu K, Lopez-Pajares V, Hollmig ST, Khavari PA (2015) CALML5 is a ZNF750- and TINCR-induced protein that binds stratifin to regulate epidermal differentiation. *Genes Dev* 29: 2225–2230

Tan EJ, Olsson AK, Moustakas A (2015) Reprogramming during epithelial to mesenchymal transition under the control of TGFbeta. *Cell Adh Migr* 9: 233–246

Tirosh I, Izar B, Prakadan SM, Wadsworth 2nd MH, Treacy D, Trombetta JJ, Rotem A, Rodman C, Lian C, Murphy G *et al* (2016a) Dissecting the multicellular ecosystem of metastatic melanoma by single-cell RNA-seq. *Science* 352: 189–196

Tirosh I, Venteicher AS, Hebert C, Escalante LE, Patel AP, Yizhak K, Fisher JM, Rodman C, Mount C, Filbin MG *et al* (2016b) Single-cell RNA-seq supports a developmental hierarchy in human oligodendroglioma. *Nature* 539: 309–313

Vandamme N, Berx G (2014) Melanoma cells revive an embryonic transcriptional network to dictate phenotypic heterogeneity. *Front Oncol* 4: 352

Verastegui C, Bille K, Ortonne JP, Ballotti R (2000) Regulation of the microphthalmia-associated transcription factor gene by the Waardenburg syndrome type 4 gene, SOX10. *J Biol Chem* 275: 30757–30760

Verfaillie A, Imrichova H, Atak ZK, Dewaele M, Rambow F, Hulselmans G, Christiaens V, Svetlichnyy D, Luciani F, Van den Mooter L *et al* (2015) Decoding the regulatory landscape of melanoma reveals TEADS as regulators of the invasive cell state. *Nat Commun* 6: 6683

Vivas-Garcia Y, Falletta P, Liebing J, Louphrasitthiphol P, Feng Y, Chauhan J, Scott DA, Glodde N, Chocarro-Calvo A, Bonham S *et al* (2020) Lineage-restricted regulation of SCD and fatty acid saturation by MITF controls melanoma phenotypic plasticity. *Mol Cell* 77: 120–137.e9

Wang X, Guo B, Li Q, Peng J, Yang Z, Wang A, Li D, Hou Z, Lv K, Kan G *et al* (2013) miR-214 targets ATF4 to inhibit bone formation. *Nat Med* 19: 93–100

Webster DE, Barajas B, Bussat RT, Yan KJ, Neela PH, Flockhart RJ, Kovalski J, Zehnder A, Khavari PA (2014) Enhancer-targeted genome editing selectively blocks innate resistance to oncokinase inhibition. *Genome Res* 24: 751–760

Wek RC, Cavener DR (2007) Translational control and the unfolded protein response. *Antioxid Redox Signal* 9: 2357–2371

Widmer DS, Hoek KS, Cheng PF, Eichhoff OM, Biedermann T, Raaijmakers MI, Hemmi S, Dummer R, Levesque MP (2013) Hypoxia contributes to

melanoma heterogeneity by triggering HIF1alpha-dependent phenotype switching. *J Invest Dermatol* 133: 2436−2443

Wilkerson MD, Hayes DN (2010) ConsensusClusterPlus: a class discovery tool with confidence assessments and item tracking. *Bioinformatics* 26: 1572−1573

Woods K, Pasam A, Jayachandran A, Andrews MC, Cebon J (2014) Effects of epithelial to mesenchymal transition on T cell targeting of melanoma cells. *Frontiers in oncology* 4: 367

Wortel IMN, van der Meer LT, Kilberg MS, van Leeuwen FN (2017) Surviving stress: modulation of ATF4-mediated stress responses in normal and malignant cells. *Trends Endocrinol Metab* 28: 794−806

Xiao Z, Zou Q, Liu Y, Yang X (2016) Genome-wide assessment of differential translations with ribosome profiling data. *Nat Commun* 7: 11194

Ye J, Kumanova M, Hart LS, Sloane K, Zhang H, De Panis DN, Bobrovnikova-Marjon E, Diehl JA, Ron D, Koumenis C (2010) The GCN2-ATF4 pathway is critical for tumour cell survival and proliferation in response to nutrient deprivation. *EMBO J* 29: 2082−2096

Zhou J, Wan J, Shu XE, Mao Y, Liu XM, Yuan X, Zhang X, Hess ME, Bruning JC, Qian SB (2018) N(6)-methyladenosine guides mRNA alternative translation during integrated stress response. *Mol Cell* 69: 636−647

Zipser MC, Eichhoff OM, Widmer DS, Schlegel NC, Schoenewolf NL, Stuart D, Liu W, Gardner H, Smith PD, Nuciforo P *et al* (2011) A proliferative melanoma cell phenotype is responsive to RAF/MEK inhibition independent of BRAF mutation status. *Pigment Cell Melanoma Res* 24: 326−333